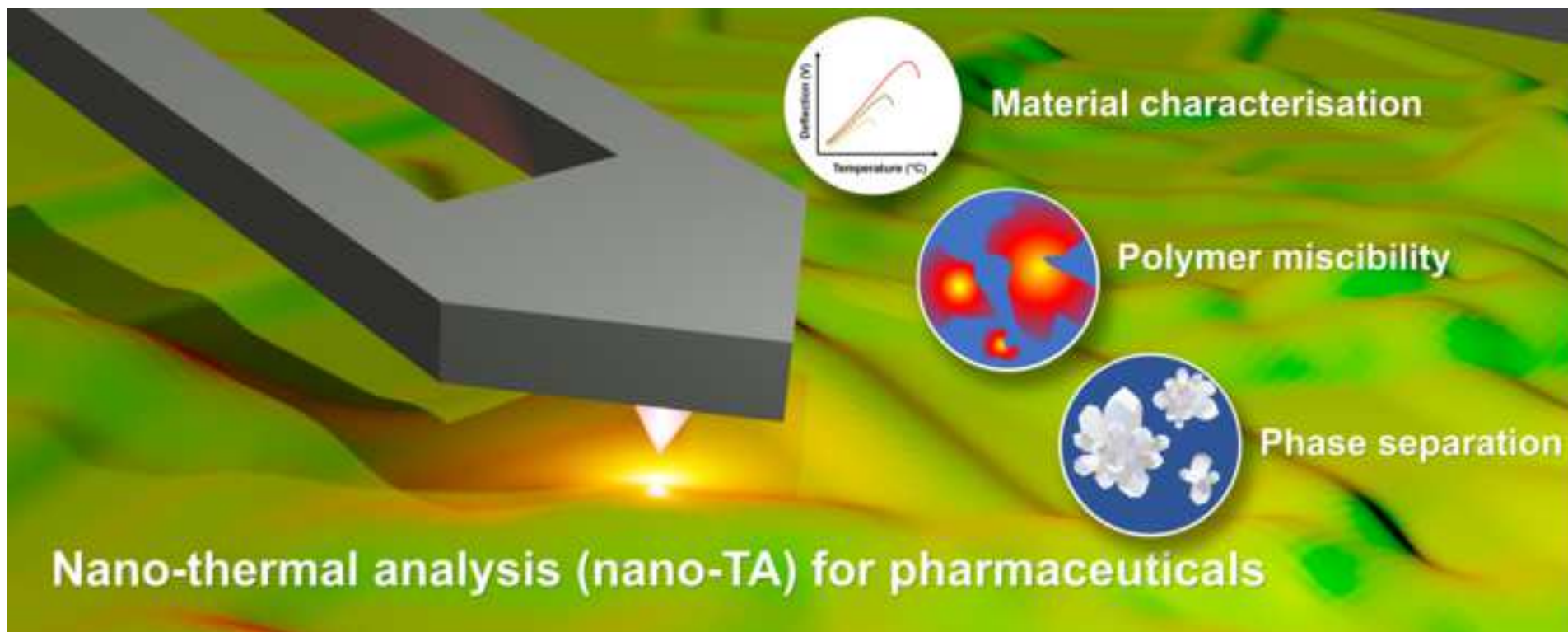# Advanced Drug Delivery Reviews

Advanced structural characterisation of pharmaceuticals using nano-thermal analysis (nano-TA)

--Manuscript Draft--

Manuscript Number:	ADDR-D-21-00214R1
Article Type:	VSI: Nanoscopy
Keywords:	Localised thermal analysis; Nano-TA; IR nanospectroscopy; Drug crystallinity; Miscibility; Pharmaceutical stability
Corresponding Author:	Majella Eileen Lane, Ph.D. University College London UNITED KINGDOM
First Author:	Choon Fu Goh, Ph.D.
Order of Authors:	Choon Fu Goh, Ph.D.
	Majella Eileen Lane, Ph.D.
Abstract:	The production of drug delivery systems fabricated at the nano scale comes with the challenges of identifying reliable characterisation tools, especially for solid dosage forms. A full understanding of physicochemical properties of solid-state systems at a high spatial resolution is essential to monitor their manufacturability, processability, performance (dissolution) and stability. Nano-thermal analysis (nano-TA), a hybrid of atomic force microscopy (AFM) and thermal analysis, has emerged as a solution to address the need for complete characterisation of samples with surface heterogeneity. Nano-TA provides not only physical information using conventional AFM but also the thermal behaviour of these systems as an additional chemical dimension. In this review, the principles and techniques of nano-TA are discussed with emphasis on recent pharmaceutical applications. Building on nano-TA, the combination of this approach with infrared spectroscopic analysis is briefly introduced. The challenges and considerations for future development of nano-TA characterisation are also outlined.

Advanced structural characterisation of pharmaceuticals using nano-thermal analysis (nano-TA)

SI: Advanced nanoscopy for physicochemical characterisation of pharmaceuticals, biologics and polymers

Choon Fu Goh[1]*, Majella E Lane[2]*

[1] Discipline of Pharmaceutical Technology, School of Pharmaceutical Sciences, Universiti Sains Malaysia, 11800 Minden, Penang, Malaysia

[2] Department of Pharmaceutics, UCL School of Pharmacy, 29-39 Brunswick Square, London WC1N 1AX, United Kingdom
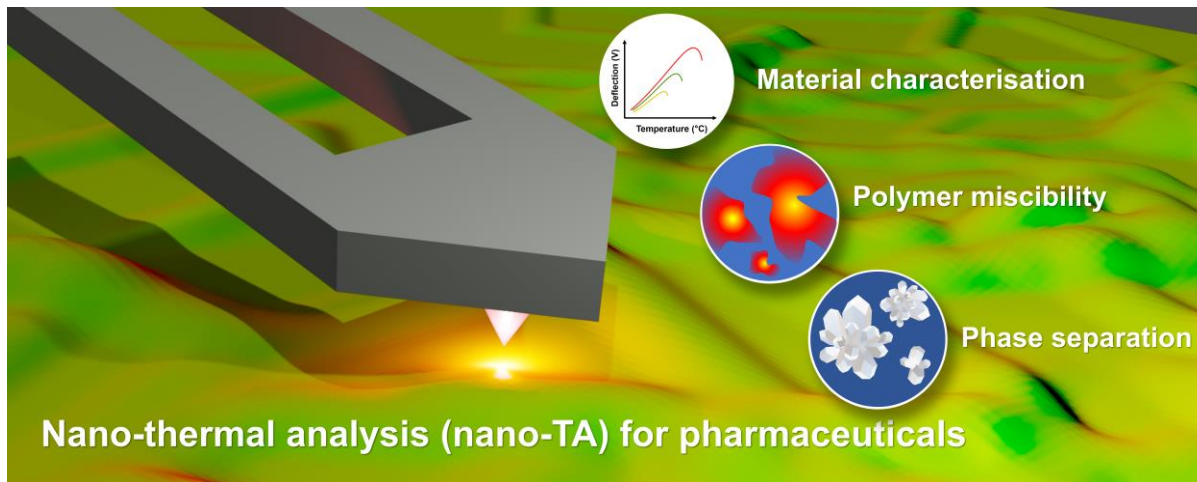
*Correspondence:

Choon Fu Goh, Discipline of Pharmaceutical Technology, School of Pharmaceutical Sciences, Universiti Sains Malaysia, 11800 Minden, Penang, Malaysia. email: choonfugoh@usm.my.

Majella E Lane, Department of Pharmaceutics, UCL School of Pharmacy, 29-39 Brunswick Square, London WC1N 1AX, United Kingdom. email: m.lane@ucl.ac.uk.

Highlights

- Solid state pharmaceutical characterisation is important for processing and performance of drug delivery systems

- Nano-TA is capable of resolving the solid state pharmaceutical characterisation of multiple components

- Nano-TA provides high spatial resolution and information on transition temperatures

- Material and phase identification forms the basis of nano-TA characterisation

Graphical abstract

Nano-thermal analysis (nano-TA) for pharmaceuticals

2

Abstract

The production of drug delivery systems fabricated at the nano scale comes with the challenges of identifying reliable characterisation tools, especially for solid dosage forms. A full understanding of physicochemical properties of solid-state systems at a high spatial resolution is essential to monitor their manufacturability, processability, performance (dissolution) and stability. Nano-thermal analysis (nano-TA), a hybrid of atomic force microscopy (AFM) and thermal analysis, has emerged as a solution to address the need for complete characterisation of samples with surface heterogeneity. Nano-TA provides not only physical information using conventional AFM but also the thermal behaviour of these systems as an additional chemical dimension. In this review, the principles and techniques of nano-TA are discussed with emphasis on recent pharmaceutical applications. Building on nano-TA, the combination of this approach with infrared spectroscopic analysis is briefly introduced. The challenges and considerations for future development of nano-TA characterisation are also outlined.

Keywords:

Localised thermal analysis; Nano-TA; IR nanospectroscopy; Drug crystallinity; Miscibility; Pharmaceutical stability

Abbreviation

AFM: Atomic force microscopy

FTIR: Fourier transform infrared

HAS: High amylose starch

HPMC: Hydroxypropyl methylcellulose

HPMCAS: hydroxypropyl methylcellulose acetate succinate

IR: infrared

Nano-TA: nano-thermal analysis/nano-localised thermal analysis

PAA: Poly(acrylic acid)

PLGA: Poly(lactic-co-glycolic acid)

PTMS: Photothermal microspectroscopy

PVP: Polyvinylpyrrolidone

PVPVA: Polyvinylpyrrolidone/vinyl acetate

T_g: Glass transition

T_gs: Softening temperature

TTM: Transition temperature microscopy

XRD: X-ray diffraction

Outline

1. Introduction

Characterisation of drugs and related delivery systems is of utmost importance for the pharmaceutical industry to understand critical properties of the formulation and also to allow continuous monitoring of manufacturing processes. Such an understanding at a fundamental level is key to unraveling the quality attributes of formulations including the stability and processing characteristics of pharmaceuticals during formulation development. At present, analytical investigation that probes the response of drug delivery systems to detail the behaviour of formulations and the related components is routine towards provision of a comprehensive understanding of the physical and chemical properties of formulations. A plethora of analytical techniques such as thermal, mechanical, microscopic, spectroscopic measurements or a combination thereof is nowadays part of the toolbox of formulation scientists to extract important information about pharmaceuticals. For solid dosage forms, knowledge of the interactions between the drug and excipients provides information concerning the compatibility, uniformity and stability of the formulation. Such interactions will influence the inherent properties of solid drugs including particle size, morphology, degree of crystallinity and polymorphism and ultimately formulation efficacy.

Currently available techniques such as thermal analysis (differential scanning calorimetry), Fourier transform infrared (FTIR) spectroscopy, Raman spectroscopy, electron microscopy and X-ray diffraction (XRD) can relate formulation performance to the fundamental properties of solid dosage forms. Unfortunately, the majority of these techniques can only provide information on "bulk" properties of materials. For example, it is not possible to apply some of these techniques including XRD to detect very low drug content and to distinguish phase-separated domains in certain products. Phase separation is a common physical instability issue for most solid dispersions, especially involving hygroscopic polymers. Under a humid atmosphere, drug may recrystallise and remain as a separate domain from a miscible polymeric system and the anticipated performance of the dosage form may be compromised, namely the drug release [1, 2]. While drug dissolution and solubility are known to be critical to the effectiveness and performance of solid pharmaceuticals, the surface physicochemical information of a solid dosage form is also extremely important as it is the the interface with the body fluids. Apart from being an indicator of product performance, surface properties should be monitored during pharmaceutical processing such as granulation,

6

tableting and coating as well as to investigate batch-to-batch variations [3]. Modification of the surface properties of a formulation can also be the first indication of altered product stability including drug recrystallisation and polymorphism. Even though conventional microscopic analysis can map the surface morphology of solid pharmaceuticals, approaches for spatially resolved analysis at the nano scale are still lacking.

Probe-based microscopy or atomic force microscopy (AFM) is an important tool that can unravel complex morphological properties of solid pharmaceuticals. It might be argued that the very high spatial resolution of AFM imaging with a cantilever with a very sharp tip does provide adequate mechanical and physical information of the surface properties of samples. However the capability of AFM to discriminate the materials via chemical identity is lacking. The hybrid of AFM and thermal analysis or thermal AFM can offer an attractive analytical strategy to characterise micro- and nano-scale heterogeneity and the compositional nature of solid pharmaceuticals. By substituting the conventional AFM tip with a thermally heated probe, this emerging localised thermal analysis technique, especially nano-localised thermal analysis (nano-TA) can elucidate the thermal properties of materials with enhanced spatial resolution (sub 100 nm for nano-TA) compared with scanning thermal microscopy (usually 1 µm); the latter was first developed by Wickramasinghe and colleagues [4, 5]. Thermal imaging that maps the thermal properties of a specific area of a product's surface can provide critical insights into the visualisation of material distribution. This is an exciting advantage over the contour differentiation and surface discontinuity that is typical of AFM topography.

This review aims to provide a perspective on thermal AFM techniques, especially nano-TA applications for solid state characterisation of pharmaceuticals. We dedicate a significant discussion to applications in pharmaceutical characterisation including identifying materials and drug phases, studying polymer miscibility and phase separation. The extension of AFM with spectroscopic analysis, especially infrared (IR) spectroscopy represents a compelling new technique providing rich potential for complementary chemical analysis and this will also be highlighted.

7

2. Techniques and principles

Scanning probe microscopy (SPM), branching from scanning tunnelling microscopy, works by using a fine probe tip to scan the sample surface, resulting in topographical characterisation data and localised force data. Examination at the atomic level allows access to electronic state and high spatial resolution data. However, this technique only characterises the physical properties of a substrate. The alliance of thermal analysis with SPM enables a comprehensive detailing of physical and chemical states of materials. This resulted in the development of thermal AFM to determine the local transition temperature of a substrate. This technique, working at the nano scale, is termed localised nano-TA. This section, hence, provides a brief overview of the working principles of AFM and nano-TA. The discussion of the techniques and applications of AFM for pharmaceuticals is not intended to be exhaustive of the field as it has been documented extensively in several other reviews [6, 7].

2.1. Atomic force microscopy

As a technique that was derived from SPM, AFM was first introduced by Gerd Binning, Calvin F. Quate and Christoph Gerber in 1986 [7, 8]. A sharp probe connected to the end of a cantilever is applied in AFM to scan the surface of samples. The movement of the probe scanning along the x-y directions is controlled by the deflection of the cantilever. This deflection in the z axis is reflected by the mutual attractive-repulsive interaction between the tip and sample [9]. Maintaining a regular deflection of the cantilever by applying a constant force to samples results in the generation of topographical images projected in three dimensions. As compared to its antecessor – STM, AFM is more versatile as it can also scan non-electrically conductive samples [8].

Different imaging modes including contact, non-contact (dynamic) and tapping have been explored to explore the surface properties of samples, especially for solid pharmaceuticals [6]. An easier way to produce the surface images is through the contact mode where a constant physical contact between the cantilever and sample exists. The repulsive van der Waals forces between the tip and sample in constant close contact is measured through the deflection of the cantilever. Owing to this intimate contact, this mode may frequently suffer from distortion and damage of the

8

cantilever, especially when the surface is stiffer than the tip. Therefore, this is ideally designed for examining smooth and rigid substances or materials in the solid state including drug crystals and polymers.

On the other hand, the non-contact mode prevents tip-sample contact and the cantilever is vibrated at a frequency close to its resonance frequency to establish attractive forces between the tip and the sample. Long range interactions such as van der Waals and electrostatic forces allow the monitoring of resonance frequency and amplitude of the cantilever when the tip approaches the sample surface. This mode can potentially generate a high resolution image because of the absence of hard contact and a minimised interaction area between the tip and the sample surface [10]. Under appropriate conditions, the image can be obtained at a true atomic resolution but this remains very challenging [11].

By combining the advantages of both contact and non-contact modes, tapping or intermittent contact modes employ an oscillating cantilever with constant repetitive contact and disengagement with the sample. Apart from generating sample topography based on height, amplitude or phase signals can be recorded for detailed surface information. In particular, phase images can show the surface contrast from the signal difference between the frequencies of the tip and oscillator. As an extension to the intermittent mode, pulsed force mode employs a sinusoidal z-modulation in mapping the sample that can simultaneously provide mechanical information such as local adhesion, elastic and electrostatic properties [12-14]. This mode has a low contact time but without lateral shear forces which are more suitable when imaging soft materials.

Apart from its use in topography, the force applied by the probe on samples can be quantified by measuring the pull off force. This force is reflected by the deflection of the cantilever when the probe is removed from contact with samples. This is useful in defining the stiffness or texture of the samples.

2.2. Localised thermal analysis

Instead of using a conventional probe, localised thermal analysis (LTA) employs a thermal probe for scanning samples, working on the same principle as AFM. The

9

thermal probe acts as a localised heating source but also functions as a miniature temperature sensor.

The Wollaston wire probe, introduced in 1994, is the earliest form of the resistive probe used for LTA by Hammiche, *et al.* [15]. The main component of the probe is a 75 µm diameter silver wire with a 5 µm platinum filament core. The wire is manipulated to form a sharp 'V' shape where the core is exposed by removing the silver electrochemically at the tip. The exposed portion is applied in LTA as a thermal sensor. Analysis using this probe is then described as microthermal analysis (µTA). ==Excellent and comprehensive reviews of the development of µTA and its applications have been published [16, 17].==

By further reducing the size of the probe, nano-TA can be achieved by using a highly doped silicon probe to achieve a high electrical resistance effect. The design analysis regarding the silicon probe for nanotopographical measurements has been discussed in detail by William [18] and Kim, *et al.* [19], enabling quantitative measurements of the probe reading in nanotopographical imaging. Incorporation of a resistive heater thermometer into an AFM cantilever by silicon doping enables electrical conduction as depicted in Fig. 1 [20]. Therefore, when a current is generated through the cantilever, more heating occurs in the lightly doped resistive heater region instead of the conductive leg which is highly doped with silicon. In order to achieve a better resolution of measurement, this silicon probe is designed to have a shorter tip, thinner cantilever, narrower leg and larger heater region than the Wollaston wire probe [18].
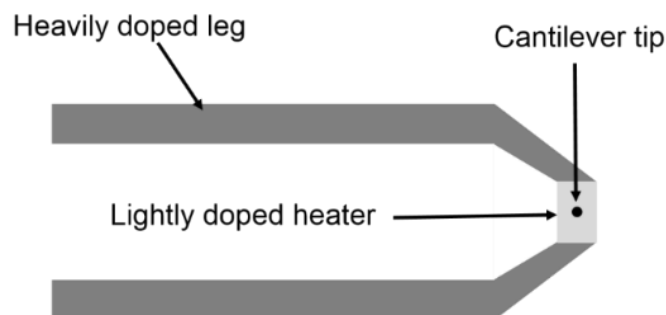
Fig. 1 Schematic representation of the silicon probe with an integrated solid-state heater that generates more heat when current flows through the cantilever

The nanotopographical metrology is conducted by recording the changes in the electrical resistance when the heated cantilever scans over a substrate with different surface contours [19]. Thermal resistance between the cantilever and the substrate increases when the cantilever tip moves away from the substrate, resulting in an increase of the cantilever temperature at a constant heating power supply. However, when the cantilever tip approaches the substrate, an increase in the thermal conductance from the cantilever causes a drop in its temperature. This temperature change in the doped silicon cantilever has been correlated with its electrical resistance [21]. Nanotopographical imaging, thus, is measured based on the differences of the cantilever electrical resistance scanning over a contoured surface.

To take full advantage of nano-TA, thermal measurements can be acquired with the resistive probe to provide calorimetric responses very close to the bulk thermal analysis. Owing to the use of a high resistance material to manufacture the tip of the probe, this allows the generation of heat with the flow of electrical current through the tip. The probe can be placed at a selected point on the sample, usually with the assistance of an optical microscope, and the probe temperature can be ramped in a similar way as for conventional thermal analysis. Probe deflection can be monitored in this case as a function of temperature that reflects the changes in the area of mechanical contact. The topographical images can also be generated with high spatial resolution based on the surface softening temperature. This is different from scanning thermal microscopy that generates image contrast based on the thermal conductivity or diffusivity. This is also one of the most typical modes of nano-TA and calibration, usually with samples of known melting points, is needed to capture the thermal exchange parameters accurately between the tip and the sample as shown in Fig. 2. Even though calibration can make temperature sensing more accurate, thermal transitions recorded may not be exactly the same (and are usually lower) as collected with bulk thermal analysis like DSC. This is usually seen in the measurements with crystals in the nanometer range or nanocrystals due to size-dependent melting temperature and entropy depression [22-25]. The melting or softening involving only the surface molecules, owing to a large ratio of the number of surface-to-volume atoms, may be the reason for this discrepancy [26].
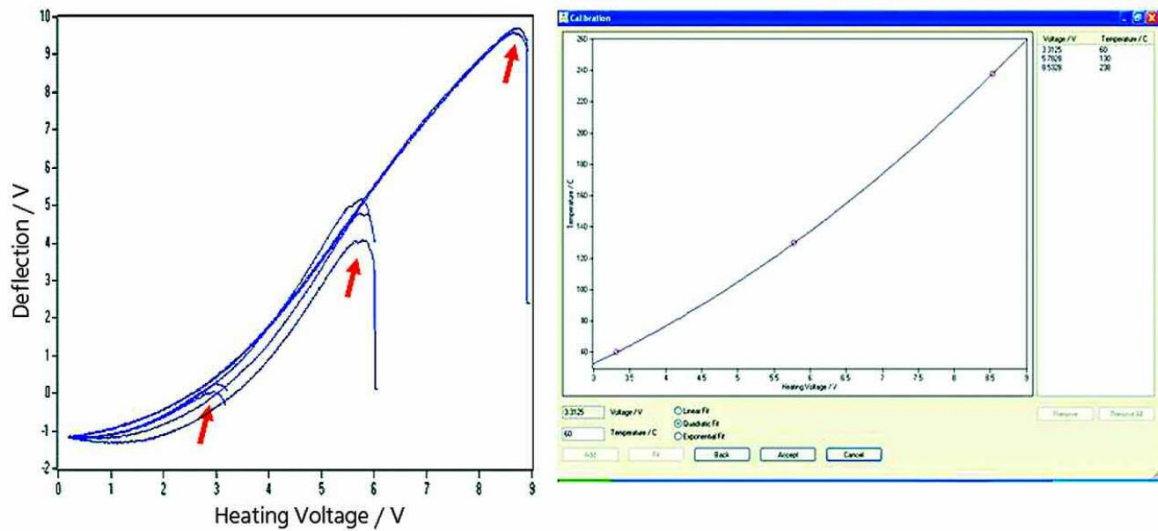
11

Fig. 2 Nano-TA data of pure calibrants including polycaprolactone (60°C), polyethylene (130°C) and polyethylene terephthalate (231°C). (Adapted from Ye, et al. [27])

Transition temperature microscopy (TTM) is an extension of the nano-TA technique and was developed based on nanotopographical thermal imaging to automatically map a specific area on a sample surface [8]. TTM enables the recording of a localised transition temperature at different points on the sample and transforms this into a TTM map in a grid pattern (Fig. 3). The transition of the temperature at each point is observed via the derivative of the displacement measurement. As the temperature of the probe increases, a positive derivative is detected due to thermal expansion but soon it drops to a negative derivative when the tip penetrates the sample. The probe is then allowed to cool after retracting from the surface. Each transition temperature is assigned a colour code and they can be collectively visualised as a blended TTM map by combining each colour pixel. Fig. 4 demonstrates the qualitative and quantitative TTM data generated from a tissue sample, porcine stratum corneum on a tape strip. The TTM map (Fig. 4C) corresponds well with the optical images (Fig. 4A and B), showing primariy two domains (purple and red). The transition temperatures for the selected pixel in each domain (Fig. 4D) are 26.1°C (purple) and 227.2°C (red), referring to the tape strip and the stratum corneum, respectively. In addition, the distribution of the transition temperatures can be tabulated in the form of a histogram (Fig. 4E) for further analysis.
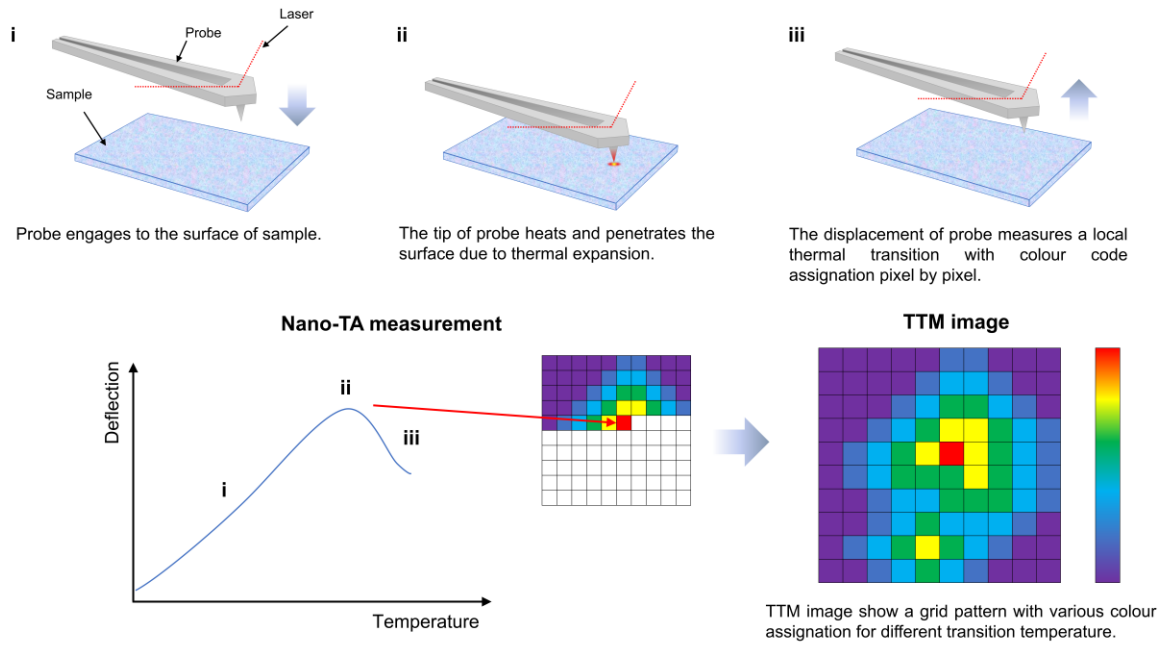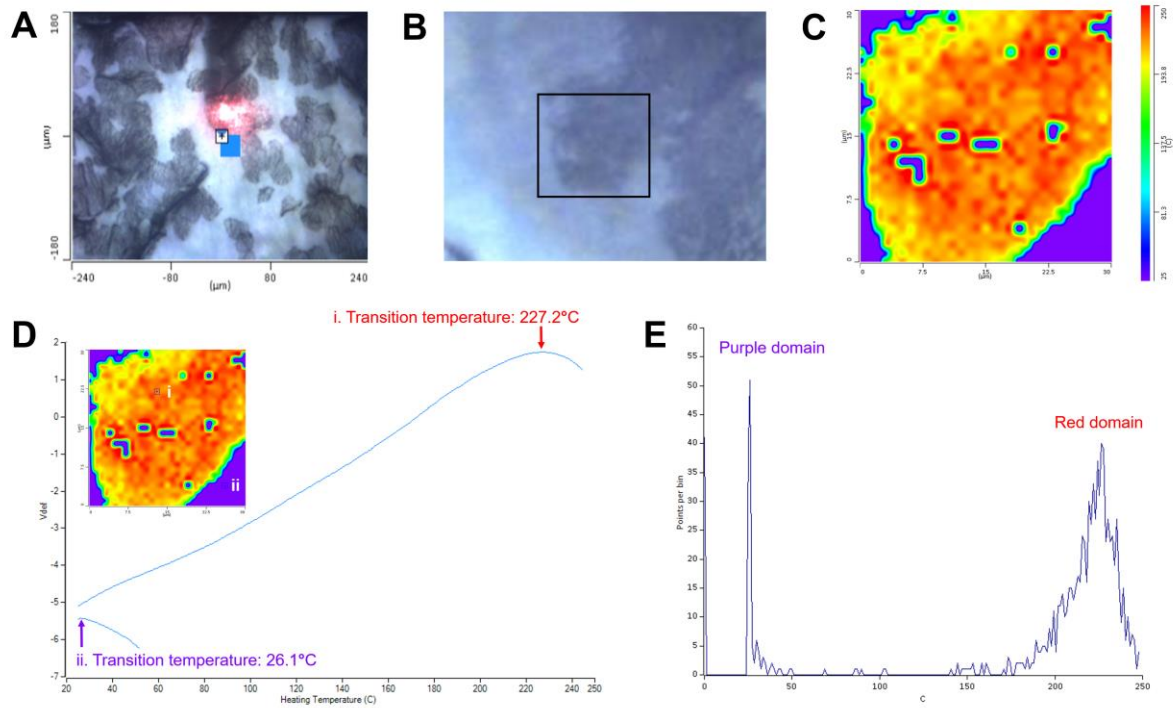
Fig. 3 The measurement of nano-TA using TTM

Fig. 4 TTM data for porcine stratum corneum on a tape strip with (A – B) optical images, (C) TTM map, (D) nano-TA measurements and (D) histograms of the map

3. Applications to pharmaceuticals

The evaluation of various pharmaceuticals, especially solid dispersions using nano-TA has been widely reported as summarised in Fig. 5. The main applications of nano-TA for pharmaceutical characterisation include material and drug phase identification, evaluation of polymer miscibility and phase separation analysis, especially of aged samples.
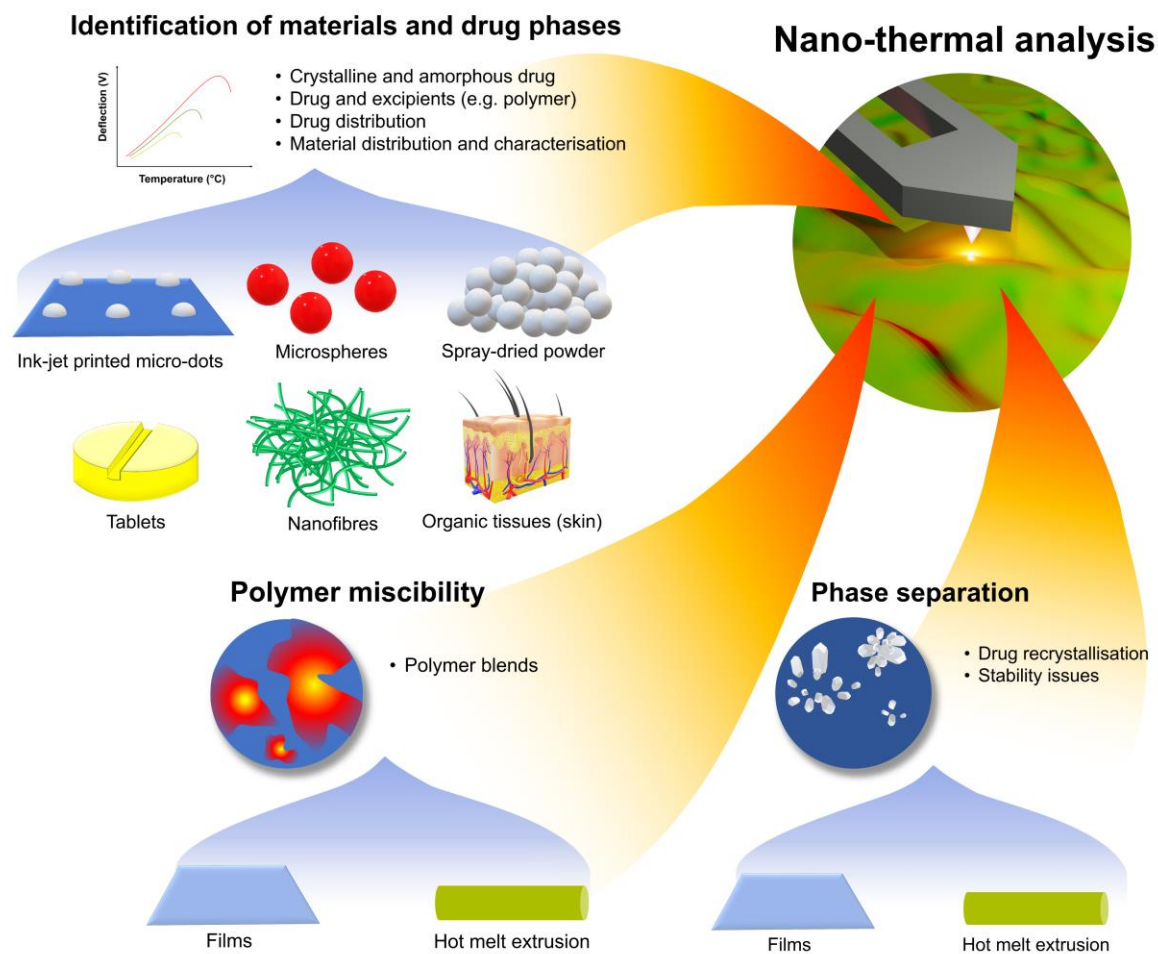

Fig. 5 Applications of nano-TA to pharmaceuticals

3.1. Identification of materials and drug phases

A pioneering study by Zhang*, et al.* [28] confirmed the ability of nano-TA to differentiate the surface heterogeneity of HPMC solid dispersions containing different loadings of carbamazepine (5 and 50%). The sample with a high drug content showed two transitions at 82°C (softening temperature, T_gs of carbamazepine) and 125°C.

Given that HPMC has a T_gs at 210°C, the latter transition is likely due to the plasticisation of carbamazepine by HPMC and this transition depression was also confirmed with DSC. For the low drug content dispersion, homogeneous samples were obtained with only a single transition at 191°C.

Scoutaris, *et al.* [29] characterised ink-jet printed micro-dot formulations of felodipine and polyvinylpyrrolidone (PVP) at various concentrations using nano-TA. There was only a single T_gs reported for all samples which reflects the homogeneity of the samples. The transition dropped from 189°C to 91°C when the drug concentration was increased from a drug/PVP ratio of 1:10 to 2:1.

Surface characterisation of spray-dried microspheres with poly(lactic-co-glycolic acid) (PLGA) and PVP K30 at different weight ratios was performed using nano-TA by Meeus, *et al.* [30]. The surface of the sample with a low PLGA:PVP ratio (20:80) showed a T_gs close to the pure PVP polymer (155°C; T_g: 174°C). When the ratio of PLGA:PVP increased to 40:60, two transitions were recorded at ~55°C and 150°C, suggesting the presence of a PLGA rich phase at the surface layer with an underlying PVP rich layer. At a higher ratio of 80:20, a transition recorded at ~10°C higher than the T_gs of pure PLGA (47°C; T_g: 39°C) was found because of a thicker PLGA shell.

Kojima, *et al.* [31] compared the distribution of nilvadipine and HPMC (50:50 ratio) in spray-dried products prepared at different nitrogen flow rates using TTM. The spray-dried products processed at a lower nitrogen flow rate of 7.5 m^3/h showed a homogenous temperature distribution with a lower softening temperature at ~70°C (T_g of nilvadipine: ~46°C). At a higher flow rate of 18.8 m^3/h, a heterogeneous temperature distribution was obtained with an additional softening temperature at ~120°C (melting temperature of nilvadipine: ~170°C), suggesting the presence of crystalline drug. However, bulk characterisation techniques including XRPD and DSC reported only amorphous material for both products.

Nakamoto, *et al.* [32] applied TTM to differentiate the crystalline ethosuximide from the corresponding amorphous counterpart on the surface of several tablet formulations with different degrees of drug crystallinity. The thermal expansion of crystalline ethosuximide resulted in a transition temperature at 37°C while the remaining ingredients including amorphous ethosuximide resulted in either no transition or transitions at a higher temperature. This specific transition was generally detected on

15

the surface of tablets with completely crystalline ethosuximide and a mixture of both crystalline (29.9 and 5.4%) and amorphous drug, except for the tablet with the lowest degree of drug crystallinity (2.5%). The results were also confirmed with Raman microspectroscopy. The TTM measurement was conducted on a larger area with a lower resolution (1000 × 1000 μm; 6 × 6 points) because of the roughness of the tablet surface.

Raimi-Abraham*, et al.* [33] identified the different materials used in the preparation of nanofibres with PVP Kollidon 90F (30%) via pressurised gyration (a technique involving simultaneous centrifugal spinning and solution blowing for fibre generation) using TTM. The average transition temperatures reported at 166.3 and 205.8°C on the TTM map refer to the T_g (156°C) and degradation temperature of PVP Kollidon 90F (200°C).

Yang*, et al.* [34] applied TTM to monitor the drug microstructure and spatial distribution within bovine serum albumin (BSA) loaded and nimodipine loaded PLGA microspheres for a better understanding of *in vitro* drug release kinetics. For BSA-PLGA microspheres, the TTM images of both microsphere surface and internal cross section displayed two main transitions at 50 - 55°C (T_gs of PLGA) and > 100°C (T_gs of BSA). A more intense region with a transition temperature > 100°C was found when the BSA loading increased from 3.66 to 8.84%. At an equal BSA loading, the interior of the microspheres had more BSA distributed than on the surface. This phenomenon explained the higher percentage of BSA release in the beginning at higher BSA content levels (6.47 and 8.84%) because of the release of bulk BSA on the surface. This was followed by a sustained release from the internal sections of the microspheres over 40 days. However, the characterisation of nimodipine-PLGA microspheres with TTM was difficult because of similar colour mapping (and similar transition temperatures; nimodipine: 60 – 90°C). The TTM maps were supported by histograms showing two major transition temperatures present at ~ 50°C and 90°C. This indicates a uniform distribution of nimodipine in the amorphous state in the PLGA matrix. A higher histogram peak was observed when the drug loading increased. The histograms also showed that the nimodipine-PLGA microspheres have a higher drug distribution in the interior of the microspheres than the surface. This observation was also confirmed at a higher nimodipine loading (22.8% vs 8.3% and 14.1%). The sustained nimodipine release from these microspheres with different drug loadings

were similar because of the control exerted by PLGA degradation. The differences in drug release behaviour between BSA and nimodipine reflected the high compatibility between nimodipine and PLGA as well as the stabilising effect of PLGA on nimodipine. The TTM data complemented the observations from MTDSC and XRD.

Goh*, et al.* [35] combined tape stripping and TTM to analyse porcine skin in order to understand the mechanism of a skin penetration enhancer, propylene glycol, as a function of depth. This was the first report of the use of nano-thermal imaging analysis to study the stratum corneum and the transition temperature detected at ~220°C reflected protein denaturation and degradation of keratin. A drop in the transition temperature of the keratin protein of the stratum corneum measured on selected tape strips was also noted, from 210 – 230 to 175 – 190°C, after treatment with propylene glycol. This may be related to the dehydration effect of PG on the keratin protein.

Following this, Goh*, et al.* [22] probed the presence of drug in the skin as solid drug crystals using tape stripping after the application of a saturated ibuprofen solution in propylene glycol as shown in Fig. 6. As well as the direct detection of the melting transition of ibuprofen drug crystals (~55°C) on the tape stripped skin samples (blue domain), TTM also allowed the indirect detection of drug crystals embedded beneath the corneocytes. This was indicated by the early penetration of the probe because of a faster melting of drug crystals beneath the layers of corneocytes, resulting in a lower transition temperature (~150°C, green domain) than the keratin protein (~220°C, red (yellow) domain). Interestingly, double transitions (Fig. 6B) consisting of firstly, the melting of tiny drug crystals (blue domain) and then a skin protein transition (red (yellow) domain) were also observed as a critical thermal event that indirectly confirmed drug crystallisation in the skin.
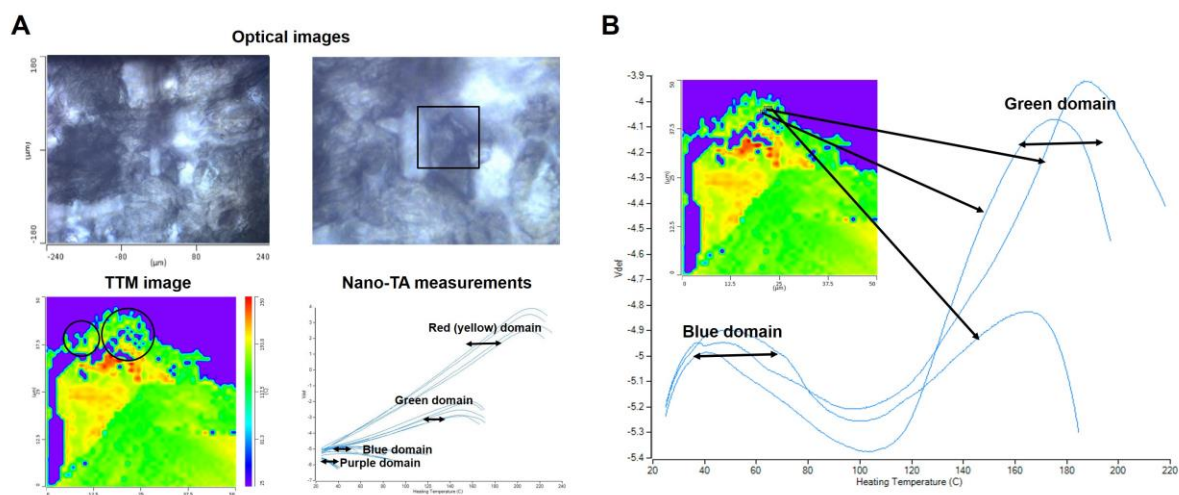
17

Fig. 6 (A) TTM data and (B) the double transitions recorded in the first tape removed after application of the saturated solution of IBU in neat PG (area: 50 × 50 μm; resolution: 1 × 1 μm). The blue domains are present in the circles of the TTM image in (A). (adapted from Goh, *et al.* [22])

Apart from nano-TA measurements, several studies by Harding, *et al.* [36] and Dai, *et al.* [37] demonstrated pulsed force imaging using a heated nanotip to discriminate the different phases of drugs (indomethacin) and excipients (lactose), respectively. The heated tip pulsed force imaging analysis allowed thermorheological measurements related to the sample stiffness (probe resistance on indentation) and adhesion (pull-off force) but the pull-off force measurement is more sensitive to detect the property changes at T_gs. Harding, *et al.* [36] observed that the pull-off force was significantly increased in the amorphous region of indomethacin at 40°C (close to the T_g of amorphous indomethacin, 43°C) as shown in Fig. 7. The increase in the pull-off force reduced gradually at a temperature above the T_g of the drug until no change was detected at 70°C when all of the drug crystallised. In subsequent work by Dai, *et al.* [37], the pull-off force was tabulated in histograms to show the power of this imaging technique to discriminate the crystalline and amorphous forms of lactose at 120°C (T_g).
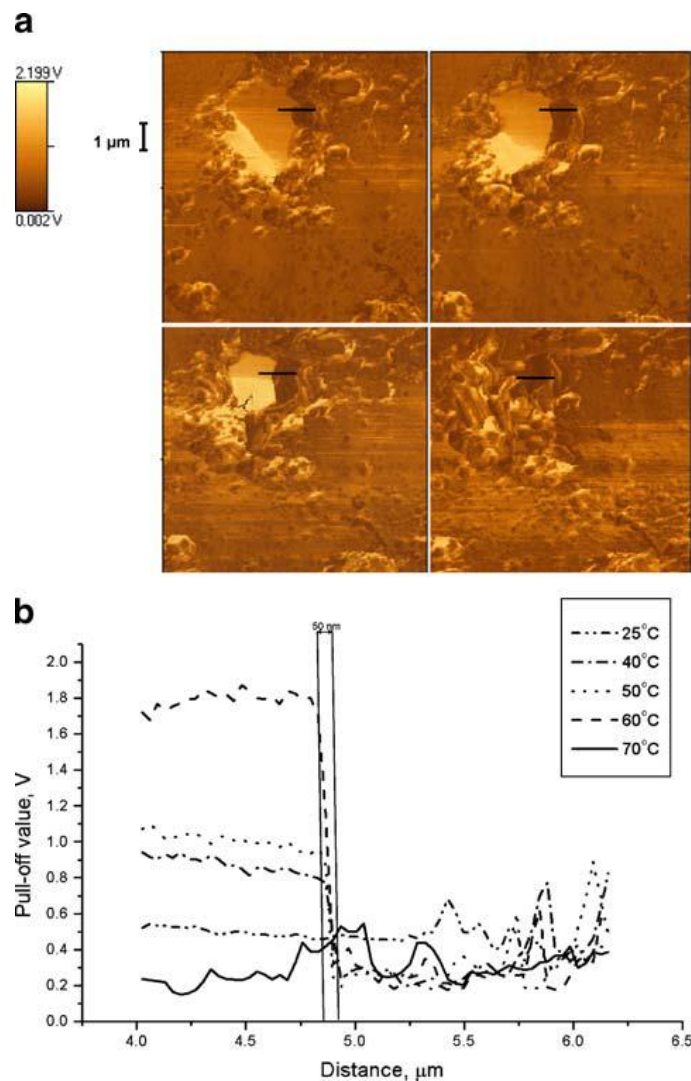
18

Fig. 7 (a) Pulsed force mode pull-off force images with heated nanotip of the indomethacin sample with an amorphous region created by heating with the thermal probe, top left 40°C, top right 50°C, bottom left 60°C, bottom right 70°C, (b) pull-off force line-scans as indicated in (a) by back horizontal lines plus data at room temperature for comparison (taken from the same region). The two vertical back lines on (b) are 50 nm apart. (adapted from Harding, *et al.* [36])

Thermally assisted nanosampling is another approach that can be manipulated to sample or transfer an extremely small amount of material [38-40]. The probe can be manipulated to pick up a particle (even femtograms) or a bulk sample on heating above the melting point. This allows the particle or sample to adhere to the probe on cooling during probe retraction before moving to another spot to deposit it with heating and rapid cooling. Such an approach was demonstrated by Harding, *et al.* [40] to deposit particles of PEG 6000 on paracetamol powder and also to study the nanointeraction of both materials through nanosampling.

3.2. Characterisation of polymer miscibility

Bisharat, *et al.* [41] characterised polymer blend films with acetylated high amylose starch (HAS) and zein at ratios of 1:3, 1:5 and 1:7 (dry weight) for tablet coating using nano-TA. HAS films showed no measurable transitions up to degradation but zein films had a softening temperature at ~75°C. The HAS-zein films showed an increase of softening temperatures from 115.7 ± 3.8, 135.9 ± 6.6 to 142.2 ± 10.4°C when the HAS:zein ratio increased. The corresponding AFM images showed a smoother surface at the highest HAS:zein ratio (1:3) but more spherical particles were found at lower HAS:zein ratios. Although the topographic inhomogeneity might indicate a different compositional distribution of the polymers, nano-TA showed only one softening transition. Given that starch and zein are immiscible, the increased softening temperature may reflect the influence of the starch on the thermomechanical properties of the films. These results were supported by FTIR analysis.

Yang, *et al.* [42] explored TTM to map the phase separation of hot melt extruded (HME) binary polymer dispersions with two immiscible polymers, Eudragit EPO and Kollidon VA 64 (PVP-VA) at 50:50 ratios. The spatial dimensions of phase separation (polymer immiscibility) were captured mainly with a long rod morphology dispersed in the continuous phase of the AFM phase image. TTM (surface and cross-section sides) showed several transitions including 100 − 110°C (T_g of PVP-VA) in the continuous phase and 40 − 50°C (T_g of Eudragit EPO) in the rod-shaped discrete phase. In addition, there were some minor areas with transitions of 65 − 85°C that correspond to the partially miscible regions of the polymers that were not observed in MTDSC analysis. This region with intermediate transitions was seen to surround mostly the Eudragit EPO region. This interesting result demonstrated the sensitivity of TTM in identifying the polymer immiscibility at the submicron or nano scale. Further studies to explore the drug loading effect (felodipine) on the binary polymer dispersions, however, were not investigated with TTM.

Tipduangta, *et al.* [43] applied nano-TA to observe phase separation of polymers in cast and spin-coated films prepared using PVP K90 and hydroxy-propyl-methylcellulose acetate succinate (HPMCAS) (1:1). The polymeric blend cast film showed continuous softening from ambient temperature similar to the spin-coated pure PVP films with a high fluidity surface. This is likely due to the phase separation of the two polymers into layers (PVP on top) as a result of slow evaporation during

20

drying. On the other hand, the spin-coated polymeric blend film showed a higher softening temperature at ~55°C that was lower than the T_g of each polymer (T_g of PVP: 176°C; HPMCAS: 122°C) and the predicted T_g of the polymer blend at the same ratio. This phenomenon may indicate less phase separation of PVP from the blend and a fraction of HPMCAS present on the film surface. Attempts were made to use nano-TA to study nanofibres of the same formulation, but the approach was unsuccessful because of the submicron dimensions of single fibres.

3.3. Understanding phase separation of drugs as an instability issue for solid dispersions

Qi, *et al.* [44] combined nano-TA and pulsed force mode AFM to characterise the low quantities of phase separation in 2-month aged felodipine and Eudragit EPO hot melt extruded (HME) samples. At higher drug loading (50%), several thermal transitions were captured on the protruded areas in the AFM images including double transitions with a softening temperature at 85°C (Eudragit EPO) and a tip penetration at 149°C (melting of crystalline felodipine form I). These thermal events indicated the coating of a felodipine crystal with a polymer layer and was supported by pulsed force mode AFM. Other point scans revealed transitions at 56 and 66°C suggesting the possibility of a mixture of amorphous drug and polymer, a mixture of amorphous/nano-crystalline drug with polymer or drug particles with a thick polymer layer. However, a softening at 59°C was recorded at a flat region similar to those found in the HME samples with low drug loadings up to 20%. This may indicate the solubilisation of submicron-sized drug crystals when the polymer was heated by the thermal probe.

With the aid of nano-TA, Zhang, *et al.* [45] examined early phase separation as an instability issue for solid dispersions of felodipine and PVP (Kollidon 30) exposed to high humidity and temperature conditions. After 3 days of exposure, AFM topography showed nanoscale heterogeneity in solid dispersions with 25%w/w of felodipine but the identification of materials was not possible. Nano-TA was employed to differentiate the felodipine and PVP rich domains (Fig. 8) with transitions at ~50°C (T_gs of felodopine, 48°C) and 200°C (T_gs of PVP, 196°C) that corresponded to the raised (brighter) and lower (darker) areas in the AFM image, respectively. This was further supported by the investigation of the localised effect caused by the heated nano-TA

21

probe. The localised features were distinctly different, especially in the PVP rich region (Fig. 9b) where a raised ring of material around the crater was observed.
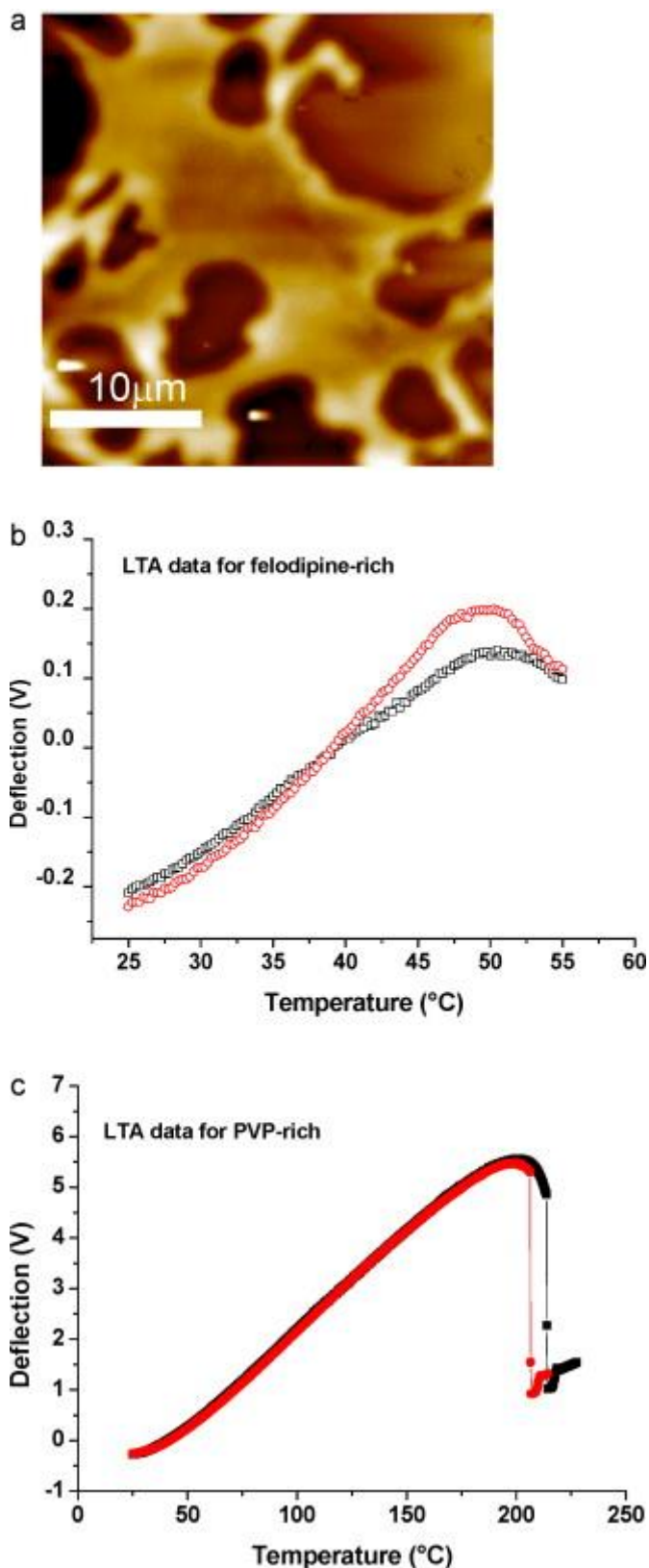
Fig. 8 (a) AFM topographic image (z scale: 400 nm) of felodipine-PVP solid dispersions (25:75 %w/w) following exposure to 75% relative humidity and 40°C for three days. (b) Nano-TA traces from the bright region in (a) determined to be felodipine-rich domains and (c) from the dark regions in (a) determined to be PVP-rich areas. (adapted from Zhang, *et al.* **[45])**
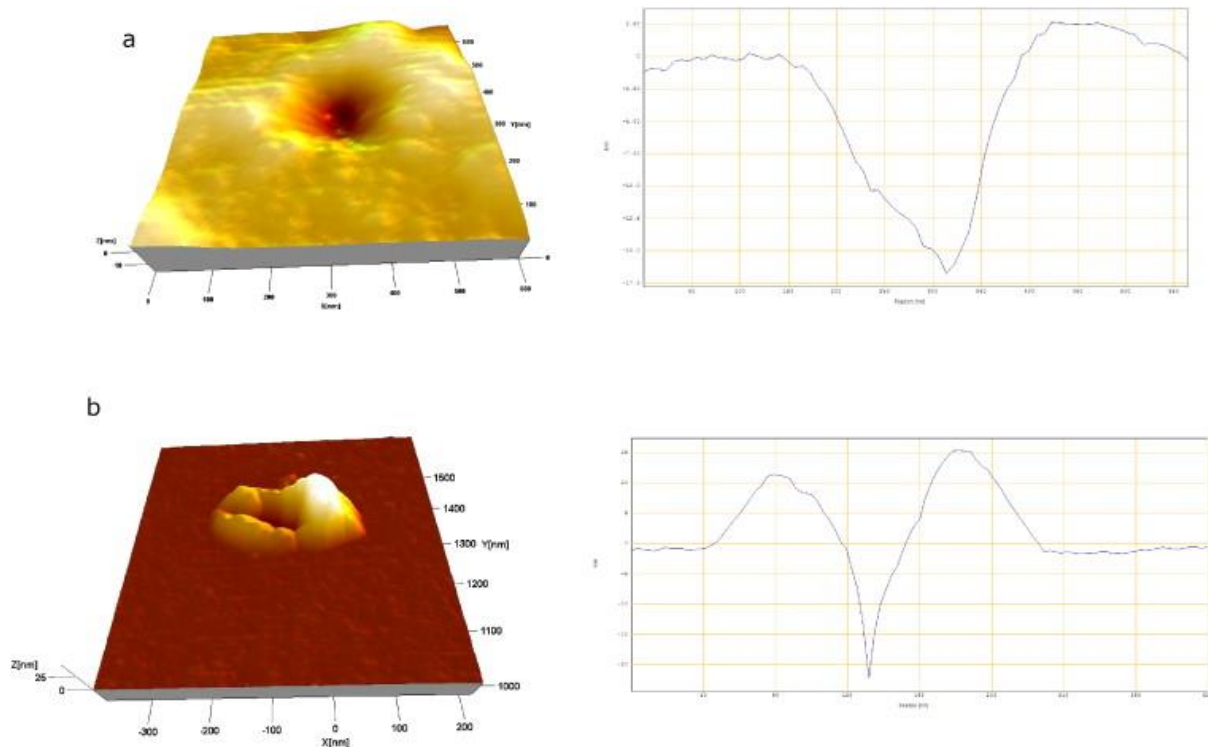
23

Fig. 9 3D 600 nm × 600 nm AFM images of indentations following a single nano-TA measurement (left) and corresponding cross-sectional profile (right) for (a) a felodipine rich region and (b) PVP rich region for felodipine-PVP solid dispersion (25:75 %w/w). (adapted from Zhang, *et al.* [45])

Following this, Qi, *et al.* [46] also studied the early phase separation (on the surface) of solid dispersion thin films of felodipine in PVP K29/32 (at 1:1 ratio) when subjected to high humidity using TTM. Prior to the investigations on the solid dispersion, spin-coated drug films were also investigated to understand the recrystallisation behaviour of felodipine alone. The freshly prepared drug film (fresh film) showed a single transition at ~ 40°C in the TTM map, representing the T_g of the amorphous felodipine. After exposing the film to high humidity for 24 h, an additional domain was reported in the TTM image at ~85°C, representing the interphase of mixed amorphous and crystalline felodipine. Double transitions (~40 and ~100°C) were noted at the interface between the amorphous and crystalline drug regions. This indicates the double layer configuration of the aged film with amorphous felodipine layering on top of crystalline felodipine of any polymorphs. The felodipine crystallinity was also confirmed by ATR-FTIR spectroscopic and microscopic data. For the solid dispersion, the fresh film showed a single transition at ~93°C that correlated well with the calculated glass

24

transition of a similar dry molecular dispersion. However, the aged film showed phase separation behaviour by showing various domains with transition temperatures at 40 − 45, 52 − 57 and 60 − 65°C. This was attributed to different drug concentrations that behaved differently with moisture uptake capacity. This hypothesis was confirmed with dynamic vapour sorption studies of the same films and TTM imaging of the films with drug-top-polymer-bottom and polymer-top-drug-bottom configurations. It must be highlighted that TTM is very sensitive to phase separation differences at the nano scale whereas AFM alone and XRD showed no major difference between the fresh and aged films.

Yang, *et al.* [47] further investigated the effect of processing (solvent based – spin coating and melting based methods – HME) on the surface crystallisation of 10-month aged amorphous molecular dispersions of felodipine and Eudragit EPO using nano-TA. In the aged HME extrudates with 10 – 70% of drug loadings, the surface showed two transitions at ~60°C (continuous) and ~90°C (discrete). The transition of the continuous phase represents the T_g of the amorphous drug dispersion (T_gs of amorphous felodipine: 42°C; Eudragit EPO: 85°C) while the transition of the discrete phase is related to the melting of crystalline felodipine under the influence of the polymer (T_gs of crystalline felodipine: 123°C). Double transitions (first: 60 – 65°C; second: 92°C) were also detected on the surface of some samples, indicating the crystalline drug underneath the amorphous drug dispersion layer. However, the cross-sections for all HME samples revealed only a single transition recorded repetitively at 53 – 60°C, indicating that amorphous dispersions remained inside the aged extrudates. Considering this finding, surface crystallisation was speculated to arise from the layer underneath the surface with a tendency to grow upwards. On the other hand, in the aged spin-coated samples, phase separation was noted on the sample surface with drug loadings of 50% and more. At 10% and 30%, only single transitions at 75°C and 83°C were reported, respectively, representing a homogenous single phase system with amorphous drug dispersion. At 50%, amorphous-amorphous phase separation was noticed with two transitions at 45°C and 65°C corresponding to the amorphous molecular dispersion and amorphous drug rich domains. Two transitions were also observed for 70% and 90% but at 60°C and 102°C, indicating phase separation of crystalline felodipine from the amorphous dispersion.

Moffat, *et al.* [48] combined nano-TA and TTM to investigate the influence of processing temperature (110 or 150°C) and residence time (5 or 15 min) on hot melt HME solid dispersions with 50%w/w of cyclosporine A in a water-miscible polymer, Eudragit EPO. The processing temperatures selected were higher (150°C) or lower (110°C) than the T_g of cyclosporine A at 126.1°C. For HME systems prepared at 110°C for 5 min, the heterogeneous sample surface resulted in a wide distribution of transition temperatures (30 – 110°C, peaking at ~70°C) in the TTM image. However, for the system prepared at 150°C for 5 min, AFM images showed a smooth surface with occasional detection of particles. The corresponding nano-TA analysis reported a major thermal event at ~90°C (T_g of drug-polymer mixture at 50:50 %w/w) with some transitions at ~120°C (T_g of cyclosporine A). Even though the TTM map showed a narrower distribution of transition temperatures than the system formed at 110°C, it is still considered broad (30 – 110°C, peaking at ~70°C). Whilst bulk thermal (MTDSC) and spectroscopic (FTIR) investigations revealed a homogenous (single phase) system for this sample, nano-TA and TTM are advantageous for detection of phase separation at the micrometer level. When the residence time was extended to 15 min, the inhomogeneity issue was resolved with a narrow distribution of transition temperatures at ~75 – 80°C on the TTM map.

Li, *et al.* [49] investigated phase-separated thin films of telaprevir in different polymers including hydroxypropyl methylcellulose (HPMC), hydroxypropyl methylcellulose acetate succinate (HPMCAS) and polyvinylpyrrolidone/vinyl acetate (PVPVA) using nano-TA. The discrete regions with a softening temperature at 124 – 130°C (close to the T_g of telaprevir by DSC: 103°C) for both HPMC and HPMCAS systems correspond to the drug rich phase in the amorphous state. The continuous phase for the corresponding systems recorded at 156°C and 143°C was assigned to the polymer rich phase. The nano-TA measurement for this polymer phase resembles the softening temperature of pure HPMCAS at 151°C but not for HPMC as the transition was much higher for pure HPMC (209°C). A lowered transition for nano-TA for this system indicates the partial miscibility of telaprevir and HPMC due to the plasticisation effect of amorphous telaprevir. However, the transitions for both discrete and continuous phases are similar for PVPVA systems owing to the similar T_g of both materials.

More recently, Li*, et al.* [50] used nano-TA to gain an in-depth understanding of the influence of the subtle microstructural phase separation of lopinavir-HPMC amorphous solid dispersions on drug release performance at different drug loadings. The group prepared the films at 33% of drug loading with the addition of water or by storing miscible films under high humidity to induce phase separation. On storing at high humidity, continuous phases and spherical-shaped discrete phases were observed on the aged miscible films with local transitions at 170 – 190°C and 80 – 140°C in nano-TA analysis, respectively (Fig. 10). The two phases corresponded to polymer rich and drug rich phases. Further investigations were carried out to study the effect of water added to the solvent during film preparation. The discrete phase had a transition at <110°C for all systems comprising mostly a drug rich domain but the continuous phase showed a drop in the transition when more than 50% of water was added. This transition drop is also comparable to the rise in the drug concentration in the corresponding T_gs measurement by nano-TA on miscible films at different drug loadings. This increased drug content also resulted in reduced drug release. An analysis of the distribution of transition measurements in different phases revealed additional phases including the polymer rich (T_gs > 150°C; 10 – 40%) and intermediate phases (105 < T_gs < 150°C; 20 – 40%) for systems prepared with 2 – 8% of water. For samples with 10 – 40% of water, a faster dissolving polymer rich phase (40 – 60%) was detected. These results supported the improved drug release with an increasing amount of water up to 40% of water addition. For another analysis comparing the impact of drug loadings (15, 33 and 50%), a high quantity of water addition could induce phase separation that actually improved drug release for higher drug loadings (33 and 50%). On closer examination of the aged miscible films, nano-TA revealed that the distribution of the polymer rich phase was the highest (close to ~40%) followed by intermediate (30 – 35%), drug rich (close to ~40%) and the polymer richest phases (~10%; T_gs: > 200°C) for both 15% and 33% drug loadings. The presence of the polymer rich phase that can improve drug release explained an enhanced drug release of aged samples with 33% drug loading but a similar drug release for 15% drug loading as its fresh samples. However, the trend changed at 50% drug loading where the majority of the transitions were the drug rich phase (> 40%). Despite having a high proportion of drug rich phase, this actually limited the extent of drug release enhancement and resulted in a lower drug release as compared with 33% drug loading.
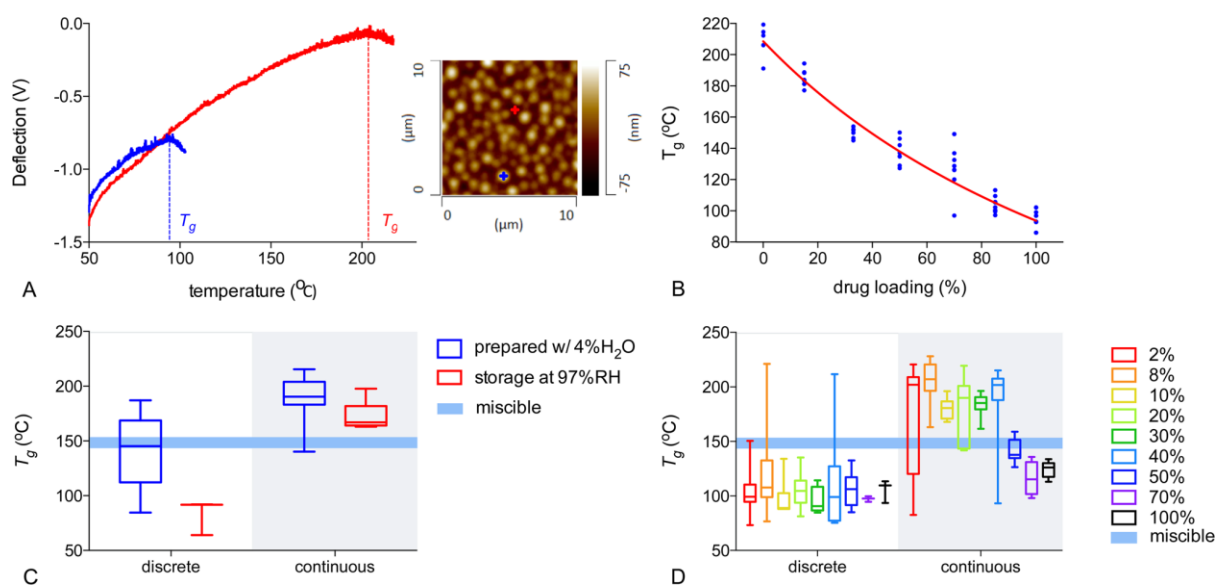
27

Fig. 10 Nano-TA characterisation of ASD films. (A) Representative nano-TA thermograms showing the local glass transition temperatures on a phase-separated amorphous solid dispersion film containing 33% lopinavir and prepared with 4% water in the solvent. (B) Glass transition temperatures obtained by nano-TA on miscible amorphous solid dispersion films at different drug loadings (red line: Gordon−Taylor fitting). (C,D) Local T_gs of continuous and discrete phases in 33% lopinavir amorphous solid dispersion films. For D, the legend shows the amount of water added to the solvent during film preparation. (adapted from Li*, et al.* [50])

4. Beyond nano-TA

Nano-TA has emerged as an excellent characterisation tool for pharmaceuticals because it combines the spatial resolution of AFM with thermal analysis. However, there are limitations to nano-TA including problems with surface roughness and differentiation of materials with similar softening temperatures. A hybrid technology combining chemical analysis of spectroscopy namely IR spectroscopy and AFM has been developed to resolve the drawbacks of nano-TA and to discriminate materials based on chemical composition.

IR nanospectroscopy is an extension of thermal AFM that employed the IR laser from a conventional Fourier Transform Infrared (FTIR) spectrometer as a heating source to induce temperature changes in the proximity of a probe tip. This interface creates a photothermal expansion of the sample to generate an oscillation or a signal from the probe that is similar to a conventional IR spectrum. AFM measurement with IR

28

spectroscopy was first developed by Hammiche, *et al.* [51] in 1999 (and Anderson [52] in 2000 separately) and this used a conventional FTIR spectrometer equipped with a broadband thermal source. Later, Hammiche and colleagues improved the setup with tuneable pulsed infrared laser produced by an optical parametric generator that greatly reduced the acquisition time but with an improved signal-to-noise ratio [53].

The early version of AFM-based IR was photothermal microspectroscopy (PTMS) coupled with Wollaston wire thermal probes for microthermal analysis. PTMS opens up the possibility of submicron spatial resolution for solid state characterisation of pharmaceuticals that complements the typical topographical profile and thermomechanical data from nano-TA [22, 38, 40, 44, 46, 54-56]. Fig. 11 demonstrates thermally assisted nanosampling of ibuprofen crystals by the Wollaston wire probe (photomicrograph) and the resemblance of the photothermal signal to the typical attenuated total reflectance (ATR) FTIR spectrum. Recent AFM-based IR systems can achieve a higher spatial resolution by applying a nanocantilever. This resolves the low brilliance of thermal IR sources and spatial resolution limit of FTIR microspectroscopy that is usually in the range of 2.5 − 75 µm (some devices attain up to 1 µm) [57].
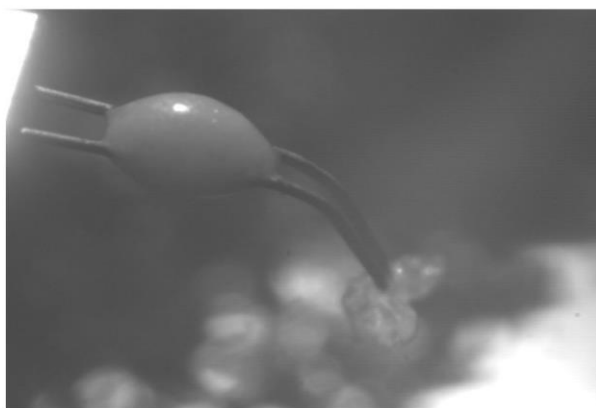
Photomicrograph

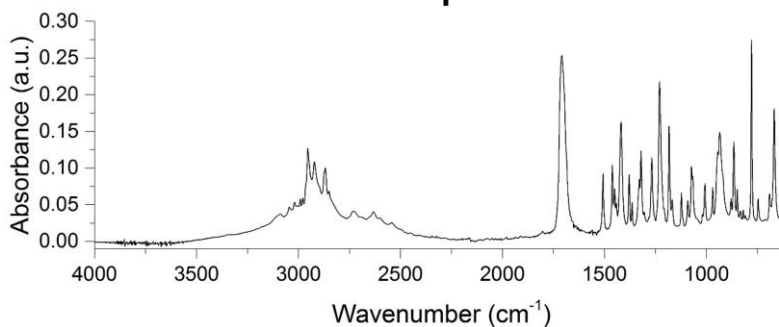**Photothermal FTIR spectrum**
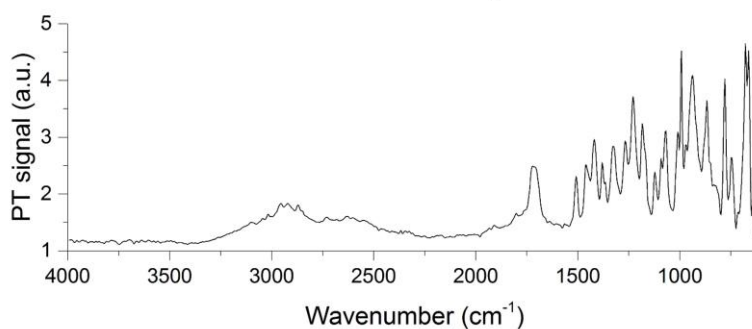
ATR-FTIR spectrum

Fig. 11 Photomicrograph showing thermally assisted nanosampling of ibuprofen crystals and the comparison of corresponding photothermal FTIR spectrum with a conventional ATR-FTIR spectrum (PT: photothermal)

Apart from the typical point scans to identify key IR peaks, IR nanospectroscopy can unambiguously map chemical content by selecting a single wavenumber or the ratio of different wavenumbers (usually comparing to a constant absorption band). Van Eerdenbrugh, *et al.* [58] compared the single wavenumber image at 1500 cm^{-1} and 1700 cm^{-1} as well as the ratio image of these two selected wavenumbers for felodipine and poly(acrylic acid) (PAA) blends (50:50) as shown in Fig. 12. The imaging at the

30

selected wavenumbers had a pattern that corresponded to the AFM topography. However, the ratio image provided better discrimination of the felodipine rich regions (green and red) and the continuous phase (blue) of polymer rich regions. Essentially, the ratio of the 1500:1700 cm^{-1} band of felodipine is smaller for the crystalline form than the amorphous counterparts. Monitoring of the presence of the single band at 1500 cm^{-1} alone is insufficient to rule out the possibility of phase separation. The ratio image however provides critical insights into the discrete distribution of materials.
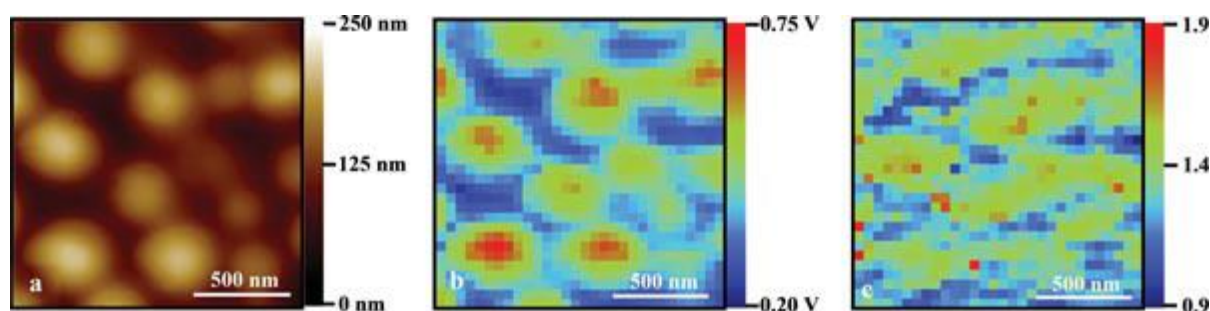

Fig. 12 IR nanospectroscopic mapping of a 50:50 (w/w) felodipine–PAA system (1.5 × 1.5 µm^2): from left to right: topographical image (color scale is 250 nm), spectroscopic image obtained at 1500 cm^{-1} (color scale is 0.20 – 0.75 V) and 1500:1700 cm^{-1} ratio image (color scale is 0.9 – 1.9). (adapted from Van Eerdenbrugh, et al. [58])

The ability to measure and map the distribution of chemical components at the nano scale has enabled the use of IR nanospectroscopy as a complementary technique to identify and characterise different phases of drugs and materials (inclusive of organic materials e.g. bacteriophages) in pharmaceutical systems including nanoparticles and liposomes [49, 59-66]. IR nanospectroscopy has also been applied to study phase separation of polymeric solid dispersions [58, 67] and miscibility of pharmaceutical blends (polymer-polymer and drug-polymer) [68-70]. Despite this, there are potential shortcomings when using IR nanospectroscopy in nanocharacterisation studies including morphological variations (height and roughness), sample thickness, a slow scanning rate (high resolution mapping), difficulties in probing soft and sticky materials as well as disturbance of surface moisture and water content [71].

5. Challenges and considerations for nano-TA characterisation

The sophisticated technique of nano-TA characterisation has advanced our understanding of the complicated surface interactions of materials and facilitates prediction of solid state stability of pharmaceuticals. Nevertheless, it remains challenging to extend the approach to meet growing needs, especially for high throughput industrial applications. The enhanced spatial resolution with thermal data offered by this method is generally compromised by long data acquisition times, fragility of the nanoprobes and lack of automation of operations.

With a typical heating rate of 10°C/s (a cooling rate of 100°C/s and a data acquisition rate of 20 point/s), a total of 22.5 s is needed to complete the recording of a full nano-TA measurement within the calibrated temperature range from 25 to 250°C. However, a shorter time period is possible if the thermal events generally happen at a lower temperature. Moffat, *et al.* [48] reported an experimental time of 15 h for TTM with an area of 50 × 50 μm and a resolution of 1 × 1 μm. With the same resolution, Goh, *et al.* [22] also observed that a scanning time ranging from 10 − 15 min was needed for an area of 10 × 10 μm and 60 − 90 min for an area of 50 × 50 μm. Likewise, Li, *et al.* [49] conducted analysis for 43 min to map an area of 4 × 4 μm with a co-average number of 8 × and resolution value of 256 pt for IR nanospectroscopy. While high resolution mapping is usually preferred, it is likely to be time consuming to map several areas to obtain a desired image. This issue may be minimised by scanning an area of interest with rapid mapping of lower resolution (> 10 × 10 μm) before selecting a higher resolution. Alternatively, a narrower temperature range may be used if the thermal events at specific temperatures are anticipated.

While a long scanning time may be expected, the characterisation may be further challenged by the sample morphology. At present, a rough and undulant surface remains a huge impediment for most AFM related techniques and nano-TA is not excluded. The nanoprobes are prone to damage usually when the initial position is not adjusted to a sufficient height from the sample surface. Even though an optical microscope is installed to assist in locating the probe from the top view, such probe adjustment from the side view is impossible but can be estimated by the naked eye for probe height adjustment. However, physically processed or assembled preparations such as tablets have potential surface defects such as gaps or valleys created when compacting the particles or powders. This presents a major

disadvantage for nano-TA measurement that may create a defect on the thermal map or destroy the probes, especially the presence of a deep gap. Damage to the probe may be avoided by selecting a lower resolution such as 200 µm for an area of 1000 × 1000 µm as reported by Nakamoto, *et al.* [32]. Probe damage may also be expected if the sample is too sticky on heating or if the probe is contaminated with other materials. Routine cleaning of nanoprobes by dipping in organic solvents such as methanol can be performed to avoid contamination with sample residues and to maintain the accuracy of subsequent sample measurements.

Nano-TA measurements can be done easily for a sample larger in size than the nanoprobe such as films and microparticles. Nevertheless, it is much more challenging to map samples of submicron or nano dimensions such as nanofibres. Raimi-Abraham, *et al.* [33] attempted to map nanofibres (diameter: 971.0 ± 517.3 nm) with 30% PVP (Kollidon 90F) using TTM but the image generated as shown in Fig. 13 does not show a clear distinctive feature of nanofibres. In another investigation of nanofibers by Tipduangta, *et al.* [43], nano-TA was reported to be unreliable and extremely difficult due to the comparatively smaller diameter of samples (0.41 ± 0.22 and 1.38 ± 0.47 µm) than reported previously.
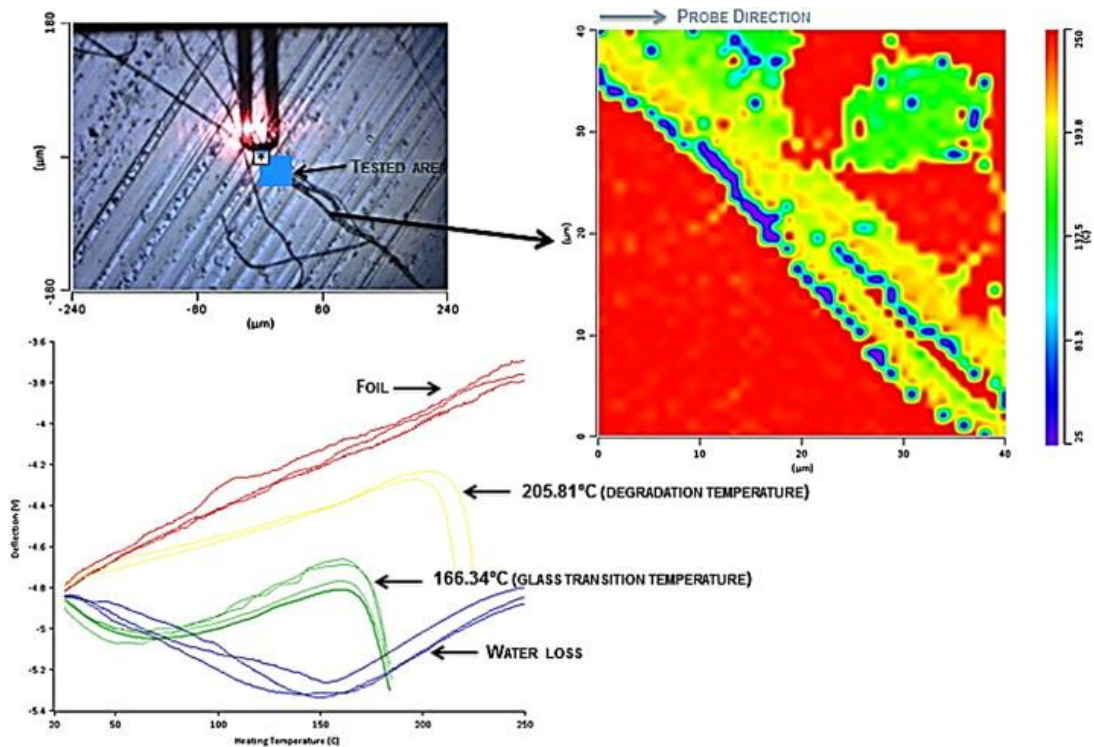
Fig. 13 Apparatus and results for TTM conducted on K90F 30% fibres. Top left image is a top-down photograph of the nano-thermal probe showing the tested area. The red halo seen on the probe is from the laser which is used to measure the probe deflection. Right image is a thermal map generated from experiment. Bottom left image shows the nano-TA profiles corresponding to transitions observed in thermal map. (adapted from Raimi-Abraham, _et al._ [33])

In most cases the problem of sample surface may be perceived as the main issue during nano-TA measurements. Owing to the destructive nature of the method, nano-TA can create defects on the sample surface on heating. Zhang, _et al._ [45] observed a raised ring of material around the crater after the area was heated by a nanoprobe as shown in Fig. 9. This feature ranged from a size of 300 – 600 nm in diameter. Attention must be paid to avoid repeating scanning on the same region or conducting repetitive single nano-TA measurements on the same spot or region. This may not reflect the true event as the heat supplied to the surrounding region may have changed the nature of the materials. It is important to allow some distance e.g. 1 µm in between the measurements. Thus, it is not surprising that a typical TTM mapping has the lowest resolution of 1 × 1 µm.

6. Conclusions

Nanoscale heterogeneity with differential surface chemistry and solid-state properties has challenged our understanding of solid state pharmaceuticals. AFM has evolved to be an emerging powerful tool to monitor the material surface at the nanoscale, but this technique is mainly limited to the sample physical and mechanical properties. Hybridisation of AFM with thermal analysis, especially nano-TA can add an extra dimension of chemical information by providing unequivocal identification of different materials at the nanoscale. This is the focus of the current review and examples of promising results from the pharmaceutical research field with nano-TA applications are highlighted.

The current nano-TA applications concentrated on resolving the puzzles of both the heterogeneous surface and inner structure of solid pharmaceutical systems, on the basis of material and interphase differentiations. These include drug crystallinity, polymorphism and drug-excipient interactions in a typical multiple component system for pharmaceuticals. This review also addresses the practical issues and considerations that facilitate nano-TA characterisations for solid pharmaceuticals. However, obstacles still remain for progression of these approaches to high-throughput applications, especially in industry. Nevertheless, the current landscape and achievements with nano-TA hold promise that further applications for this technique will emerge in the future.

Declaration of interest:

The authors have no relevant affiliations or financial involvement with any organisation or entity with a financial interest in or financial conflict with the subject matter or materials discussed in the manuscript. This includes employment, consultancies, honoraria, stock ownership or options, expert testimony, grants or patents received or pending, or royalties.

Acknowledgments:

None

REFERENCES

[1] A.C.F. Rumondor, L.A. Stanford, L.S. Taylor, Effects of Polymer Type and Storage Relative Humidity on the Kinetics of Felodipine Crystallization from Amorphous Solid Dispersions, Pharm Res, 26 (2009) 2599.

[2] A.C.F. Rumondor, L.S. Taylor, Effect of Polymer Hygroscopicity on the Phase Behavior of Amorphous Solid Dispersions in the Presence of Moisture, Mol. Pharm., 7 (2010) 477-490.

[3] E. Hadjittofis, M.A. Isbell, V. Karde, S. Varghese, C. Ghoroi, J.Y.Y. Heng, Influences of Crystal Anisotropy in Pharmaceutical Process Development, Pharm Res, 35 (2018) 100.

[4] J.M.R. Weaver, H.K. Wickramasinghe, Semiconductor characterization by scanning force microscope surface photovoltage microscopy, Journal of Vacuum Science & Technology B: Microelectronics and Nanometer Structures Processing, Measurement, and Phenomena, 9 (1991) 1562-1565.

[5] C.C. Williams, H.K. Wickramasinghe, Scanning thermal profiler, Applied Physics Letters, 49 (1986) 1587-1589.

[6] A. Kaur, D.P. Kale, A.K. Bansal, Surface characterization of pharmaceutical solids, TrAC Trends in Analytical Chemistry, 138 (2021) 116228.

[7] Y.T.A. Turner, C.J. Roberts, M.C. Davies, Scanning probe microscopy in the field of drug delivery, Advanced Drug Delivery Reviews, 59 (2007) 1453-1473.

[8] X. Dai, J.G. Moffat, J. Wood, M. Reading, Thermal scanning probe microscopy in the development of pharmaceuticals, Advanced Drug Delivery Reviews, 64 (2012) 449-460.

[9] A. Diaspro, R. Rolandi, Atomic force microscopy [Guest Editorial], Engineering in Medicine and Biology Magazine, IEEE, 16 (1997) 26-27.

[10] D. Johnson, N. Hilal, Characterisation and quantification of membrane surface properties using atomic force microscopy: A comprehensive review, Desalination, 356 (2015) 149-164.

[11] F.J. Giessibl, Atomic Resolution of the Silicon (111)-(7×7) Surface by Atomic Force Microscopy, Science, 267 (1995) 68-71.

[12] H.-U. Krotil, T. Stifter, H. Waschipky, K. Weishaupt, S. Hild, O. Marti, Pulsed force mode: a new method for the investigation of surface properties, Surface and Interface Analysis, 27 (1999) 336-340.

[13] A. Rosa-Zeiser, E. Weilandt, S. Hild, O. Marti, The simultaneous measurement of elastic, electrostatic and adhesive properties by scanning force microscopy: pulsed-force mode operation, Measurement Science and Technology, 8 (1997) 1333-1338.

[14] T. Miyatani, M. Horii, A. Rosa, M. Fujihira, O. Marti, Mapping of electrical double-layer force between tip and sample surfaces in water with pulsed-force-mode atomic force microscopy, Applied Physics Letters, 71 (1997) 2632-2634.

[15] A. Hammiche, M. Reading, H.M. Pollock, M. Song, D.J. Hourston, Localized thermal analysis using a miniaturized resistive probe, Review of Scientific Instruments, 67 (1996) 4268.

[16] H.M. Pollock, A. Hammiche, Micro-thermal analysis: techniques and applications, Journal of Physics D: Applied Physics, 34 (2001) R23.

[17] M. Reading, D.M. Price, D.B. Grandy, R.M. Smith, L. Bozec, M. Conroy, A. Hammiche, H.M. Pollock, Micro-thermal analysis of polymers: current capabilities and future prospects, Macromolecular Symposia, 167 (2001) 45-62.

[18] P.K. William, Design analysis of heated atomic force microscope cantilevers for nanotopography measurements, Journal of Micromechanics and Microengineering, 15 (2005) 2441.

[19] K.J. Kim, K. Park, J. Lee, Z.M. Zhang, W.P. King, Nanotopographical imaging using a heated atomic force microscope cantilever probe, Sensors and Actuators A: Physical, 136 (2007) 95-103.

[20] B.W. Chui, T.D. Stowe, J. Yongho Sungtaek, K.E. Goodson, T.W. Kenny, H.J. Mamin, B.D. Terris, R.P. Ried, D. Rugar, Low-stiffness silicon cantilevers with

37

integrated heaters and piezoresistive sensors for high-density AFM thermomechanical data storage, Journal of Microelectromechanical Systems, 7 (1998) 69-78.

[21] B.W. Chui, M. Asheghi, Y.S. Ju, K.E. Goodson, T.W. Kenny, H.J. Mamin, Intrinsic-carrier thermal runaway in silicon microcantilevers, Microscale Thermophysical Engineering, 3 (1999) 217-228.

[22] C.F. Goh, J.G. Moffat, D.Q.M. Craig, J. Hadgraft, M.E. Lane, Monitoring Drug Crystallization in Percutaneous Penetration Using Localized Nanothermal Analysis and Photothermal Microspectroscopy, Mol. Pharm., 16 (2019) 359-370.

[23] Q. Jiang, Z. Zhang, J.C. Li, Melting thermodynamics of nanocrystals embedded in a matrix, Acta Materialia, 48 (2000) 4791-4795.

[24] L.H. Liang, J.C. Li, Q. Jiang, Size-dependent melting depression and lattice contraction of Bi nanocrystals, Physica B: Condensed Matter, 334 (2003) 49-53.

[25] B.A. Jones, J.M. Torkelson, Large melting point depression of 2–3-nm length-scale nanocrystals formed by the self-assembly of an associative polymer: Telechelic, pyrene-labeled poly(dimethylsiloxane), Journal of Polymer Science Part B: Polymer Physics, 42 (2004) 3470-3475.

[26] H.M. Lu, P.Y. Li, Z.H. Cao, X.K. Meng, Size-, shape-, and dimensionality-dependent melting temperatures of nanocrystals, The Journal of Physical Chemistry C, 113 (2009) 7598-7602.

[27] J. Ye, M. Reading, N. Gotzen, G. Van Assche, Scanning thermal probe microscopy: nanothermal analysis with Raman microscopy., Microscopy and Analysis, 21 (2007) S5-S8.

[28] J. Zhang, M. Bunker, X. Chen, A.P. Parker, N. Patel, C.J. Roberts, Nanoscale thermal analysis of pharmaceutical solid dispersions, Int J Pharm, 380 (2009) 170-173.

[29] N. Scoutaris, M.R. Alexander, P.R. Gellert, C.J. Roberts, Inkjet printing as a novel medicine formulation technique, J. Control. Release, 156 (2011) 179-185.

[30] J. Meeus, X. Chen, D.J. Scurr, V. Ciarnelli, K. Amssoms, C.J. Roberts, M.C. Davies, G.v. Den Mooter, Nanoscale Surface Characterization and Miscibility Study of a Spray-Dried Injectable Polymeric Matrix Consisting of Poly(lactic-co-glycolic acid) and Polyvinylpyrrolidone, J. Pharm. Sci., 101 (2012) 3473-3485.

[31] Y. Kojima, T. Ohta, K. Shiraki, R. Takano, H. Maeda, Y. Ogawa, Effects of spray drying process parameters on the solubility behavior and physical stability of solid dispersions prepared using a laboratory-scale spray dryer, Drug Development and Industrial Pharmacy, 39 (2012) 1484-1493.

[32] K. Nakamoto, T. Urasaki, S. Hondo, N. Murahashi, E. Yonemochi, K. Terada, Evaluation of the crystalline and amorphous states of drug products by nanothermal analysis and Raman imaging, Journal of Pharmaceutical and Biomedical Analysis, 75 (2013) 105-111.

[33] B.T. Raimi-Abraham, S. Mahalingam, M. Edirisinghe, D.Q.M. Craig, Generation of poly(N-vinylpyrrolidone) nanofibres using pressurised gyration, Mater. Sci. Eng. C, 39 (2014) 168-176.

[34] F. Yang, D. Chen, Z.-f. Guo, Y.-m. Zhang, Y. Liu, S. Askin, D.Q.M. Craig, M. Zhao, The application of novel nano-thermal and imaging techniques for monitoring drug microstructure and distribution within PLGA microspheres, Int J Pharm, 522 (2017) 34-49.

[35] C.F. Goh, J.G. Moffat, D.Q.M. Craig, J. Hadgraft, M.E. Lane, Nano-thermal imaging of the stratum corneum and its potential use for understanding of the mechanism of skin penetration enhancer, Thermochim Acta, 655 (2017) 278-283.

[36] L. Harding, W. King, X. Dai, D.M. Craig, M. Reading, Nanoscale characterisation and imaging of partially amorphous materials using local thermomechanical analysis and heated tip AFM, Pharm Res, 24 (2007) 2048-2054.

[37] X. Dai, M. Reading, D.Q.M. Craig, Mapping amorphous material on a partially crystalline surface: Nanothermal analysis for simultaneous characterisation and imaging of lactose compacts, J. Pharm. Sci., 98 (2009) 1499-1510.

[38] M. Reading, D. Grandy, A. Hammiche, L. Bozec, H.M. Pollock, Thermally assisted nanosampling and analysis using micro-IR spectroscopy and other analytical methods, Vibrational Spectroscopy, 29 (2002) 257-260.

[39] X. Dai, J.G. Moffat, A.G. Mayes, M. Reading, D.Q.M. Craig, P.S. Belton, D.B. Grandy, Thermal probe based analytical microscopy: Thermal analysis and photothermal Fourier-transform infrared microspectroscopy together with thermally

assisted nanosampling coupled with capillary electrophoresis, Analytical Chemistry, 81 (2009) 6612-6619.

[40] L.J. Harding, M. Reading, D.Q.M. Craig, The development of thermally assisted particle manipulation and thermal nanointeraction studies as a means of investigating drug-polymer interactions, J. Pharm. Sci., 97 (2008) 1551-1563.

[41] L. Bisharat, S.A. Barker, A. Narbad, D.Q.M. Craig, In vitro drug release from acetylated high amylose starch-zein films for oral colon-specific drug delivery, Int J Pharm, 556 (2019) 311-319.

[42] Z. Yang, K. Nollenberger, J. Albers, D. Craig, S. Qi, Microstructure of an Immiscible Polymer Blend and Its Stabilization Effect on Amorphous Solid Dispersions, Mol. Pharm., 10 (2013) 2767-2780.

[43] P. Tipduangta, P. Belton, L. Fábián, L.Y. Wang, H. Tang, M. Eddleston, S. Qi, Electrospun Polymer Blend Nanofibers for Tunable Drug Delivery: The Role of Transformative Phase Separation on Controlling the Release Rate, Mol. Pharm., 13 (2016) 25-39.

[44] S. Qi, P. Belton, K. Nollenberger, A. Gryczke, D.Q.M. Craig, Compositional Analysis of Low Quantities of Phase Separation in Hot-Melt-Extruded Solid Dispersions: A Combined Atomic Force Microscopy, Photothermal Fourier-Transform Infrared Microspectroscopy, and Localised Thermal Analysis Approach, Pharm Res, 28 (2011) 2311-2326.

[45] J. Zhang, M. Bunker, A. Parker, C.E. Madden-Smith, N. Patel, C.J. Roberts, The stability of solid dispersions of felodipine in polyvinylpyrrolidone characterized by nanothermal analysis, Int J Pharm, 414 (2011) 210-217.

[46] S. Qi, J.G. Moffat, Z. Yang, Early stage phase separation in pharmaceutical solid dispersion thin films under high humidity: Improved spatial understanding using probe-based thermal and spectroscopic nanocharacterization methods, Mol. Pharm., 10 (2013) 918-930.

[47] Z. Yang, K. Nollenberger, J. Albers, J. Moffat, D. Craig, S. Qi, The effect of processing on the surface physical stability of amorphous solid dispersions, Eur. J. Pharm. Biopharm., 88 (2014) 897-908.

[48] J. Moffat, S. Qi, D.M. Craig, Spatial characterization of hot melt extruded dispersion systems using thermal atomic force microscopy methods: The effects of processing parameters on phase separation, Pharm Res, 31 (2014) 1744-1752.

[49] N. Li, L.S. Taylor, Nanoscale Infrared, Thermal, and Mechanical Characterization of Telaprevir–Polymer Miscibility in Amorphous Solid Dispersions Prepared by Solvent Evaporation, Mol. Pharm., 13 (2016) 1123-1136.

[50] N. Li, L.S. Taylor, Microstructure Formation for Improved Dissolution Performance of Lopinavir Amorphous Solid Dispersions, Mol. Pharm., 16 (2019) 1751-1765.

[51] A. Hammiche, H.M. Pollock, M. Reading, M. Claybourn, P.H. Turner, K. Jewkes, Photothermal FT-IR spectroscopy: A step towards FT-IR microscopy at a resolution better than the diffraction limit, Applied Spectroscopy, 53 (1999) 810-815.

[52] M.S. Anderson, Infrared Spectroscopy with an Atomic Force Microscope, Applied Spectroscopy, 54 (2000) 349-352.

[53] L. Bozec, A. Hammiche, H.M. Pollock, M. Conroy, J.M. Chalmers, N.J. Everall, L. Turin, Localized photothermal infrared spectroscopy using a proximal probe, Journal of Applied Physics, 90 (2001) 5159-5165.

[54] L. Harding, S. Qi, G. Hill, M. Reading, D.Q.M. Craig, The development of microthermal analysis and photothermal microspectroscopy as novel approaches to drug–excipient compatibility studies, Int J Pharm, 354 (2008) 149-157.

[55] J.G. Moffat, M.D. Eddleston, P.S. Belton, W. Jones, D.Q.M. Craig, Analysis of single particle photodegradation using photothermal infrared microspectroscopy, Analyst, 138 (2013) 2315-2322.

[56] L.C. Grisedale, J.G. Moffat, M.J. Jamieson, P.S. Belton, S.A. Barker, D.Q.M. Craig, Development of Photothermal FTIR Microspectroscopy as a Novel Means of Spatially Identifying Amorphous and Crystalline Salbutamol Sulfate on Composite Surfaces, Mol. Pharm., 10 (2013) 1815-1823.

[57] A. Dazzi, C.B. Prater, AFM-IR: Technology and Applications in Nanoscale Infrared Spectroscopy and Chemical Imaging, Chemical Reviews, 117 (2017) 5146-5173.

[58] B. Van Eerdenbrugh, M. Lo, K. Kjoller, C. Marcott, L.S. Taylor, Nanoscale Mid-Infrared Imaging of Phase Separation in a Drug–Polymer Blend, J. Pharm. Sci., 101 (2012) 2066-2073.

[59] A.J. Harrison, E.A. Bilgili, S.P. Beaudoin, L.S. Taylor, Atomic Force Microscope Infrared Spectroscopy of Griseofulvin Nanocrystals, Analytical Chemistry, 85 (2013) 11449-11455.

[60] J. Mathurin, E. Pancani, A. Deniset-Besseau, K. Kjoller, C.B. Prater, R. Gref, A. Dazzi, How to unravel the chemical structure and component localization of individual drug-loaded polymeric nanoparticles by using tapping AFM-IR, Analyst, 143 (2018) 5940-5949.

[61] C.J. Schram, S.P. Beaudoin, L.S. Taylor, Impact of Polymer Conformation on the Crystal Growth Inhibition of a Poorly Water-Soluble Drug in Aqueous Solution, Langmuir, 31 (2015) 171-179.

[62] M. Tuteja, M. Kang, C. Leal, A. Centrone, Nanoscale partitioning of paclitaxel in hybrid lipid–polymer membranes, Analyst, 143 (2018) 3808-3813.

[63] K. Wieland, G. Ramer, V.U. Weiss, G. Allmaier, B. Lendl, A. Centrone, Nanoscale chemical imaging of individual chemotherapeutic cytarabine-loaded liposomal nanocarriers, Nano Research, 12 (2019) 197-203.

[64] D. Khanal, J. Zhang, W.-R. Ke, M.M. Banaszak Holl, H.-K. Chan, Bulk to Nanometer-Scale Infrared Spectroscopy of Pharmaceutical Dry Powder Aerosols, Analytical Chemistry, 92 (2020) 8323-8332.

[65] D. Khanal, I. Khatib, J. Ruan, D. Cipolla, F. Dayton, J.D. Blanchard, H.-K. Chan, W. Chrzanowski, Nanoscale Probing of Liposome Encapsulating Drug Nanocrystal Using Atomic Force Microscopy-Infrared Spectroscopy, Analytical Chemistry, 92 (2020) 9922-9931.

[66] D. Khanal, R.Y.K. Chang, S. Morales, H.-K. Chan, W. Chrzanowski, High Resolution Nanoscale Probing of Bacteriophages in an Inhalable Dry Powder Formulation for Pulmonary Infections, Analytical Chemistry, 91 (2019) 12760-12767.

[67] S. Saboo, L.S. Taylor, Water-induced phase separation of miconazole-poly (vinylpyrrolidone-co-vinyl acetate) amorphous solid dispersions: Insights with confocal fluorescence microscopy, Int J Pharm, 529 (2017) 654-666.

[68] B. Van Eerdenbrugh, M. Lo, K. Kjoller, C. Marcott, L.S. Taylor, Nanoscale Mid-Infrared Evaluation of the Miscibility Behavior of Blends of Dextran or Maltodextrin with Poly(vinylpyrrolidone), Mol. Pharm., 9 (2012) 1459-1469.

[69] H.S. Purohit, L.S. Taylor, Miscibility of Itraconazole–Hydroxypropyl Methylcellulose Blends: Insights with High Resolution Analytical Methodologies, Mol. Pharm., 12 (2015) 4542-4553.

[70] P. Nguyen Tri, R.E. Prud'homme, Crystallization and Segregation Behavior at the Submicrometer Scale of PCL/PEG Blends, Macromolecules, 51 (2018) 7266-7273.

[71] W. Fu, W. Zhang, Hybrid AFM for Nanoscale Physicochemical Characterization: Recent Development and Emerging Applications, Small, 13 (2017) 1603525.

Legends:

Figures:

Fig. 1 Schematic representation of the silicon probe with an integrated solid-state heater that generates more heat when current flows through the cantilever

Fig. 2 Nano-TA data of pure calibrants including polycaprolactone (60°C), polyethylene (130°C) and polyethylene terephthalate (231°C). (Adapted from Ye, et al. [21])

Fig. 3 The measurement of nano-TA using TTM

Fig. 4 TTM data for porcine stratum corneum on a tape strip with (A – B) optical images, (C) TTM map, (D) nano-TA measurements and (D) histograms of the map

Fig. 5 Applications of nano-TA to pharmaceuticals

Fig. 6 (A) TTM data and (B) the double transitions recorded in the first tape removed after application of the saturated solution of IBU in neat PG (area: 50 × 50 μm; resolution: 1 × 1 μm). The blue domains are present in the circles of the TTM image in (A). (adapted from Goh, et al. [16])

Fig. 7 (a) Pulsed force mode pull-off force images with heated nanotip of the indomethacin sample with an amorphous region created by heating with the thermal probe, top left 40°C, top right 50°C, bottom left 60°C, bottom right 70°C, (b) pull-off force line-scans as indicated in (a) by back horizontal lines plus data at room temperature for comparison (taken from the same region). The two vertical back lines on (b) are 50 nm apart. (adapted from Harding, et al. [31])

Fig. 8 (a) AFM topographic image (z scale: 400 nm) of felodipine-PVP solid dispersions (25:75 %w/w) following exposure to 75% relative humidity and 40°C for three days. (b) Nano-TA traces from the bright region in (a) determined to be felodipine-rich domains and (c) from the dark regions in (a) determined to be PVP-rich areas. (adapted from Zhang, et al. [40])

Fig. 9 3D 600 nm × 600 nm AFM images of indentations following a single nano-TA measurement (left) and corresponding cross-sectional profile (right) for (a) a felodipine rich region and (b) PVP rich region for felodipine-PVP solid dispersion (25:75 %w/w). (adapted from Zhang, et al. [40])

Fig. 10 Nano-TA characterisation of ASD films. (A) Representative nano-TA thermograms showing the local glass transition temperatures on a phase-separated amorphous solid dispersion film containing 33% lopinavir and prepared with 4% water in the solvent. (B) Glass transition temperatures obtained by nano-TA on miscible amorphous solid dispersion films at different drug loadings (red line: Gordon−Taylor fitting). (C,D) Local T_gs of continuous and discrete phases in 33% lopinavir amorphous solid dispersion films. For D, the legend shows the amount of water added to the solvent during film preparation. (adapted from Li, et al. [45])

Fig. 11 Photomicrograph showing thermally assisted nanosampling of ibuprofen crystals and the comparison of corresponding photothermal FTIR spectrum with a conventional ATR-FTIR spectrum (PT: photothermal)

Fig. 12 IR nanospectroscopic mapping of a 50:50 (w/w) felodipine–PAA system (1.5 × 1.5 μm2): from left to right: topographical image (color scale is 250 nm), spectroscopic image obtained at 1500 cm−1 (color scale is 0.20 – 0.75 V) and 1500:1700 cm−1 ratio image (color scale is 0.9 – 1.9). (adapted from Van Eerdenbrugh, et al. [51])

Fig. 13 Apparatus and results for TTM conducted on K90F 30% fibres. Top left image is a top-down photograph of the nano-thermal probe showing the tested area. The red

halo seen on the probe is from the laser which is used to measure the probe deflection. Right image is a thermal map generated from experiment. Bottom left image shows the nano-TA profiles corresponding to transitions observed in thermal map. (adapted from Raimi-Abraham, et al. [28])